Direct Reactions with Exotic Nuclei

P. G. Hansen

National Superconducting Cyclotron Laboratory, Michigan State University, East Lansing, Michigan 48824; e-mail: hansen@nscl.msu.edu

and

Department of Physics and Astronomy, Michigan State University, East Lansing, Michigan 48824

J. A. Tostevin

Department of Physics, School of Electronics and Physical Sciences, University of Surrey, Guildford, Surrey GU2 7XH, United Kingdom; e-mail: J.Tostevin@surrey.ac.uk

KEYWORDS: One- and two-nucleon knockout reactions, eikonal reaction theory, stripping reactions, breakup reactions, single-particle spectroscopy, spectroscopic factors, intermediate energy, radioactive ion beams, drip line nuclei, halo nuclei.

ABSTRACT: The identification of direct reaction processes and their subsequent exploitation for the spectroscopy of weak radioactive beams of exotic nuclei is an important problem in modern nuclear physics. One- and two-nucleon knockout reactions, studied using intermediate energy radioactive beams, have now been the subject of a number of careful analyses and been shown to have the potential to contribute to this problem. This article discusses the current status of such investigations and reviews what has been learned to date from the accumulated experiments and analyses of the last five years. The techniques are still in their formative stages

and the open questions and challenges are outlined.

CONTENTS

1 INTRODUCTION

The study of short-lived radioactive nuclei far from the valley of beta stability, often referred to as "exotic nuclei", is attracting the interest of physicists worldwide. New experimental methods are under rapid development that permit studies of the structure of nuclei which lie close to the limits of nuclear existence in the N–Z plane, referred to as the drip lines, where the nucleon separation energy goes to zero. (In order to make the drip line a single-valued function it is convenient to define the neutron/proton drip lines by the lightest particle-stable nuclide within a family of isotones/isotopes.) Near the neutron drip line the large neutron excess and low neutron binding energy can lead to dramatic changes in the nuclear structure. There is good evidence that for neutron numbers 8 and 20, normally considered to represent "magic" nuclei, i.e. closed-shell structures, the shell gaps disappear at the drip line, and intruder states with opposite parity descend from the next higher shell. These may even become the ground state. In some cases, the low binding allows the wave function of one or more neutrons to extend far beyond the range of the strong force giving rise to a neutron halo, already observed in a number of light nuclei. Phenomena like these are a challenge to theory and provide a test bench for more exact solutions and an improved understanding of the nuclear many-body problem.

It may sound surprising to many that such solutions do not already exist. However, in spite of many successful insights provided by nuclear structure theory, the existing framework is still largely empirical, and is definitely so for all heavier nuclei. The reason for this is the major role played by correlations in the wave function brought about by the long-range components of the nucleon-nucleon interaction. Although the shell model sets out from a picture based on

non-interacting nucleons moving in a central field there are, in fact, only very few nuclei near double-closed shells that are directly amenable to such a simple approach. The nucleon-nucleon correlations usually make it necessary to take into account explicitly the mixing of many valence configurations. For lighter nuclei, such as those discussed in this article, it is practical to apply a microscopic description involving the diagonalization of a large matrix representing the (effective) interactions in a restricted space of single-particle orbitals. Such techniques have for some time (1) covered nuclei up to mass A=40 and recent developments, such as stochastic methods (2, 3), are now shifting the limit of calculations towards A=80–100 with high predictive power (4). There is also a major current effort to develop accurate ab-initio quantum mechanical calculations using a many-body Hamiltonian derived from the free nucleon-nucleon interaction, as determined from scattering experiments. It is indicative of the difficulty of this task that current technology, see the review of (5), may only be able to handle masses up to approximately A=12.

Nuclear correlations can be probed in a specific and quantitative way by a judicious choice of nuclear reactions that selectively excite some simple degrees of freedom. For example, Coulomb excitation has long been the preferred method for investigating collective degrees of freedom involving the motion of several or many nucleons. It has been found that this can be done very favorably with radioactive beams at intermediate energies of 30–300 MeV/nucleon (6). Perhaps the simplest degree of freedom is that associated with the single-particle orbital components that, at the microscopic level, form the correlated many-body wave function. These can best be studied using direct reaction processes that add or remove one or a few nucleons and which can identify single-particle orbitals,

their quantum numbers and their occupancies. Again it has turned out that reactions with intermediate-energy radioactive beams offer a very powerful tool; these reactions, referred to as knockout reactions, in which one or more nucleons are removed from the nuclei of the beam, are the subject of the present article.

To introduce the subject we examine in some detail a specific experiment which illustrates how knockout reactions can provide spectroscopic information. The example in Fig. 1 is taken from an extensive series of experiments (7–18) carried out at the National Superconducting Cyclotron Laboratory at Michigan State University. A detailed analysis demonstrates that the ground state of ^{17}C must have spin-parity $3/2^+$ and that the, theoretically possible, $1/2^+$ and $5/2^+$ assignments are excluded (12). Furthermore, the presence in the neutron knockout cross section populating the ^{16}C 2^+ state of orbital components of different ℓ reveals that the ^{17}C ground state has a complex structure. In simplified language, the main components may be viewed as the $1s_{1/2}$ and $0d_{5/2}$ neutron single-particle states coupled to the first excited 2^+ state of ^{16}C. The deduced ℓ=0 and 2 spectroscopic factors for these cross sections are 0.21(9) and 1.2(3), respectively, whereas theory predicts 0.16 and 1.44. (Our definitions and experimental and theoretical details will be given later in this article.)

What are the main lessons we wish to draw from this initial example? The first is that the technique is remarkably sensitive; the data in Fig. 1 were collected in about one day of measurement with an incident ^{17}C beam of intensity 100–300 particles per second (s^{-1}). The operational limit is considerably lower; in the same series of experiments (12) useful data were taken with a ^{19}C beam of only 0.5–1 s^{-1}, see Fig. 3. (Compare this with the beam intensity in a classical cyclotron or Van de Graaf experiment.) Three factors account for this high sen-

sitivity, thick targets of a fraction of a g/cm^2, strong forward focusing due to the high-energy beam, and essentially background-free event-by-event tracking. None of these advantages apply in low-energy experiments with radioactive beams. The second lesson is that the experiment furnishes significant spectroscopic information and thus provides an exacting test, in this case of the structures of the (^{17}C,^{16}C) pair. We consider it crucial that such individual and systematic spectroscopic studies start from a consistent theoretical approach. Case-by-case analyses, each using tailored parameter sets, will be of little value as experiments focus on a few powerful accelerators supplying rare and weak beams. Structure studies must involve a strong interplay between theory and experiment to the benefit of both. The third lesson, not yet substantiated by what has been said in this Introduction, but to which we will return, is that the high-energy limits of reaction theory, based on eikonal methods, offer formal, practical and quantitative advantages over conventional direct-reaction approaches. This precision offers the possibility of addressing more fundamental problems such as the physical reality of the orbitals that make up the model space of the shell-model.

The organization of this article is as follows. Section 2 gives a brief overview of the vast subject of the applications of direct reactions for nuclear spectroscopy. We also present a brief aperçu of the shell model and spectroscopic factors. We then introduce the single-nucleon knockout reaction, discuss its early applications to halo systems, and present the associated eikonal reaction theory. It is important that the eikonal model provides both a non-perturbative treatment of the projectile break-up mechanisms and an essentially parameter-free estimate of the single-particle knockout cross sections. We use as examples the spectroscopy of bound and unbound final states. In Section 4 we discuss the determination of

absolute spectroscopic factors and their relationship to the description and occupation of single-particle orbitals in a truncated model space. This latter question transcends radioactive beam research and bears on the fundamental basis of the shell model. We then discuss two very recent developments. The first is the observation that two-proton knockout from nuclei close to the neutron drip line and, conversely, two-neutron knockout at the proton drip line, must proceed as a direct reaction. This opens many new possibilities for structure and two-particle correlation studies in nuclei. The second is that knockout reactions may, in many cases, produce tertiary beams with significant spin alignment. This potentially interesting spectroscopic tool is so far unexplored. Finally we mention some of the open questions and experimental and theoretical challenges that will need to be faced in the future.

2 THE LEGACY OF SPECTROSCOPY USING DIRECT-REACTIONS

Systematic studies of nuclear reactions were essential to the development of modern nuclear physics. For this review, those direct reactions which excite selectively a minimal number of nucleonic degrees of freedom are particularly important. These provide a diagnostic for identifying the microscopic or single-particle structures of nuclei. Unable to cover this vast subject, this Section presents some of the concepts and lessons learned that are especially important to modern experimentation with radioactive beams. We do not have space to deal with the closely related subject of electromagnetic excitation, but point out that the Coulomb excitation of bound states has become an important tool in radioactive-beams research; see the review of Glasmacher (6). The Coulomb dissociation of simple, loosely bound systems also plays an important role in reactions of halo nuclei

and in astrophysics; see the reviews by Esbensen (19) and Austin (20). Even for reactions on light targets, that are the main concern of this article, in the interests of precision we will often cite the Coulomb dissociation cross section σ_C in addition to that from the nuclear breakup channels.

2.1 Transfer reactions

The high resolution offered by cyclotrons and van de Graaf accelerators permitted the development of a spectroscopy based on direct reactions and the direct measurement of excitation energies of final states. Distorted wave theories of stripping and pickup reactions (21–25), assuming two-body descriptions of both the entrance and exit channels, related the measured fragment angular distributions and nucleon ℓ values of the transfer. The partial cross sections to a given state then lead to spectroscopic factors offering (indirect) information about the single-particle occupancies in the nuclear wave function. The workhorses of this effort were the (d,p) stripping and (p,d) pickup reactions, but many other reactions were used including two-particle transfers. The role of deuteron breakup effects on the calculated angular distributions and deduced spectroscopic factors were also studied extensively (26–29) and found to be important. The adiabatic approach, in particular, clarified (26, 27) that the inclusion of breakup effects reduced the reaction's apparent sensitivity to the nuclear interior and enhanced its surface localization. Including the effects of breakup lead to much improved agreement with theoretical spectroscopic factor systematics.

The spectroscopic factor is an important quantity that links measurements to microscopic theories of nuclear structure. The concept plays an important part in what follows so we provide an outline definition here. Detailed discussions can

be found elsewhere (21–23, 30). Consider the removal of a single nucleon from an initial state of A nucleons of spin I forming a given final state of the $A-1$ nucleon residue with spin I_c. The overlap function between the initial and final state many-body wave functions carries angular momentum $|I - I_c| \leq j \leq I + I_c$ and is a function of a single spatial variable and so can be written

$$\langle \vec{r}, \Psi_f^{A-1} | \Psi_i^A \rangle = \sum_j c_j^{if} \psi_j(\vec{r}) \,, \tag{1}$$

where details of the angular momentum coupling are not shown. With the ψ_j normalized to unity, the spectroscopic factor is $\mathrm{S}_j^{if} = |c_j^{if}|^2$, usually defined to include a sum over final single-particle m values. The sum-rule value for the spectroscopic factors to all final states for a specific orbital is the average occupancy of this orbital. Hence, S_j is unity for nucleon removal from a pure single-particle state and $(2j+1)$ for nucleon removal from a filled j-subshell. In the isospin representation in which T_i and T_f of the initial and final states are specified, the spectroscopic factor is written C^2S, with C^2 the square of the isospin coupling coefficient. In principle, the one-body overlap functions can be expanded in a complete set with basis states, characterized by different radial quantum numbers n. The notation of Eq. (1) is appropriate for most practical shell-model calculations with a space typically restricted to a few j values, each with only one n. When spectroscopic factors are calculated in a harmonic-oscillator basis they require a center-of-mass motion correction (30,31). This appears as a factor $[A/(A-1)]^N$, where N=0,1,2... is the major oscillator quantum number. Often neglected, the correction is important for precise comparisons with data (17,18).

Comparisons of the theoretical and experimental cross sections for a single-nucleon removal reaction, from initial state i to a final state f of the residue, are

made assuming

$$\sigma_{th}^{if} = \sum_j \mathrm{S}_j^{if}\ \sigma_{sp}(n\ell j)\ , \tag{2}$$

where the cross sections σ_{sp} are calculated assuming a normalized nucleon-residue wave function ψ_j of given n.

In transfer reaction analyses the σ_{sp} are often computed using the distorted-waves Born approximation (DWBA), assuming optical-model two-body entrance and exit channel wave functions, or, more recently, by introducing adiabatic or coupled channels three-body wave functions to include the effects of breakup. A comprehensive survey of measured spectroscopic factors for the *sd* shell has been given by Endt (32). Such calculations each involve a significant number of potential and other parameters which are best chosen (22) from global parameter sets optimized to the systematics for a range of nuclei and beam energies. Such systematics are not available for studies in the neutron and proton rich sectors of the nuclear chart.

For reactions with radioactive beams one also has to work with inverse kinematics since the nucleus of interest is now the projectile and not the target. Interest in the halo nucleus ^{11}Be has prompted work on the p(^{11}Be,^{10}Be)d reaction at 35 MeV/nucleon by Fortier *et al.* (33,34). There are also data for the d(^{56}Ni,^{57}Ni)p reaction by Rehm *et al.* (35), but with currently available beam intensities such experiments are a significant experimental challenge. There is also an interest in applying transfer reactions to investigate (unbound) structures in the continuum. Korsheninnikov *et al.* (36) have used the p(^{8}He,^{7}He)d reaction to observe an excited state in the unbound ^{7}He residue at 2.9 MeV.

Direct proton-transfer reactions have also recently found new applications as an indirect tool for determining the rates of radiative proton capture in certain

reactions of interest to nuclear astrophysics. The method makes use of the observation that for a given ℓ, and at large distances from the nucleus, the radial form of the tail of the proton wave function is determined by the asymptotically correct Whittaker function (37). All structure information is therefore in the normalization of this tail, defined by an asymptotic normalization coefficient (ANC) C_ℓ^2, see (38) and the earlier work cited therein. For a single j value the C_ℓ is defined by equating the "true" radial wave function, expressed as the product of structure factors and the normalized radial single-particle wave function $R_\ell(r)$, with the product of C_ℓ and the Whittaker function W, the comparison being made at an asymptotic distance r_L. For a p-shell proton

$$\left(\frac{A}{A-1}\,\mathrm{S}_j\,R_s\right)^{1/2}\;R_\ell(r_L) = C_\ell\,\frac{W_{-\eta,\,\ell+\frac{1}{2}}(2kr_L)}{r_L}\;, \tag{3}$$

where η is the Sommerfeld parameter and k the bound-state wave number. The parameter R_s, to be discussed in subsection 4.1, is a correction which reduces the spectroscopic factor and arises from short-range correlation effects. A measurement of the transfer cross section will suffice to determine the ANC and thus specify the proton single-particle wave function at large distances. The method has been applied to proton capture on ^{7}Be (39) and ^{8}B (40) and has been tested in reactions on ^{16}O (41). The method exploits the highly peripheral nature of the transfer reaction at selected energies and fragment angles, thus emphasizing the far nuclear surface. The cross section is then directly correlated with the ANC. While the deduced asymptotic normalization depends less on the assumed nucleon binding potential than does the spectroscopic factor, comparisons with structure theory are very difficult since the ANC is not an output from most structure calculations. The method also cannot give guidance on the scattering wave function to be used in the calculation of the electromagnetic matrix element,

although the choice of nuclear potential used can affect the calculated capture rate appreciably (18, 42).

The high sensitivity of transfer reactions to the single-particle components in the nuclear wave function requires that the momentum transfer is matched to the momenta of the valence nucleons in the nuclear surface, typically 50–150 MeV/c. This condition is met at tandem energies. An example of what happens at higher energies is provided by a study by Smith et al. (43) of the (p,d) reaction at 800 MeV incident beam energy on a number of targets including ^{12}C and ^{16}O. With momentum transfers in the range 350–500 MeV/c the single-hole excitations were still seen, but high-spin final states became prominent and the strongest excitations observed did not correspond to known levels. The authors interpreted these as originating in multi-step processes which are favored by the high momentum transfer. This suggests that the adaptation of medium- and high-energy transfer reactions with radioactive beams as a spectroscopic tool may be of limited value for characterizing the wave function. For high-energy one-nucleon knockout reactions, to be discussed in the main part of this article, this problem does not arise: the momentum transferred is that of the struck particle, irrespective of the beam energy.

2.2 Knockout reactions: (p,2p) and (e,e′p)

Reactions such as ^{16}O(p,2p)^{15}N provided an early test of the reality of deeply bound nuclear shell structures. In this case the experiments showed, in addition the well-known $0p_{1/2}$ and $0p_{3/2}$ hole states at 0 and 6.3 MeV excitation energy, a broad peak near 30 MeV attributed to the $0s_{1/2}$ state, see the reviews (44, 45) of the (p,2p) reaction. Using proton beams of several hundred MeV, and short

wavelength, the reaction has sufficient energy to excite deep hole states and favors localized interactions, emphasizing single-particle properties. In addition, since the nucleon-nucleon cross sections are small at these energies, the reaction can be treated in the impulse approximation, i.e. as a quasi-free scattering. The experiments have typically detected the two outgoing protons in coincidence at approximately $\pm 45°$. The proton angular distribution reveals the ℓ value. Near $45°$ an s-state has a maximum while a p-state has a minimum. Let the momenta of the incoming and two outgoing protons be $\vec{k}_0$, $\vec{k}_1$, and $\vec{k}_2$. The excitation spectrum can now be obtained from the momentum balance

$$\vec{k}_{A-1} = \vec{k}_0 - \vec{k}_1 - \vec{k}_2 = -\vec{k}_3 \,, \tag{4}$$

where $\vec{k}_3$ denotes the momentum of the struck nucleon which, in the sudden approximation, is equal and opposite to that of the recoiling mass $(A-1)$ residue.

The corresponding proton knockout reaction using a beam of high-energy electrons has become extremely important for providing absolute spectroscopic factors to test the physical occupancies of the shell-model orbitals. This seemed beyond the powers of nucleon transfer reactions; thus Macfarlane and Schiffer (22) commented that while transfer reactions could provide relative spectroscopic factors, absolute values were of "very questionable meaning". The (e,e′p) reaction has been developed through the eighties and nineties into a precision tool for measuring the spectroscopic factors of proton single-particle states in well bound nuclei, see especially Kramer et al. (46). The results, for deep-hole proton states in nuclei from A=6 to 209, are that the (e,e′p) reaction measures spectroscopic factors that are lower by a factor 0.50–0.65 than those calculated in the shell model. This systematic reduction is believed to arise from the repulsive short-range part of the nucleon-nucleon interaction, see the review by Pandharipande

et al. (47). Since this hard repulsion sets in at distances below 0.4 fm, it follows from the uncertainty principle that components in the nucleon wave functions must arise with momenta of order 500 MeV/c. These components are hard to measure directly, but they become conspicuous through reduced occupancies of low-lying proton single-particle states. The comparison is here with shell model calculations based on effective interactions and model spaces which do not incorporate effects of the hard core in nucleon-nucleon scattering. A first direct confirmation of this suggestion comes from a study of the ^{7}Li(e,e′p)^{6}He reaction by Lapikas et al. (48). The combined experimental spectroscopic factor to the 0^{+} and 2^{+} states of ^{6}He was found to be 0.58(5) in excellent agreement with the value 0.60 obtained from a microscopic variational Monte-Carlo calculation based on realistic nucleon-nucleon interactions.

It now appears that similar information can be obtained for both neutron and proton single-particle states using nuclear knockout reactions, not only for those nuclei available as stable targets but quite generally for all radioactive nuclei available as fast beams. This prospect will be discussed in Section 4.

3 SINGLE-NUCLEON KNOCKOUT WITH FAST RADIOACTIVE BEAMS

The first experiments with radioactive nuclear beams were carried out more than fifty years ago (49) and the challenging problem of studying the structure of nuclei far from stability was clearly posed by 1966 (50). Nevertheless, the only experimental tools available until the beginning of the eighties were studies of radioactivity. These included measurements of decay radiation and of ground-state properties such as masses, spins, nuclear moments and of charge radii obtained

from the atomic hyperfine structure. The emergence of fast radioactive beams from the fragmentation of heavy-ions was of major importance to the field and offered the possibility of using nuclear reactions systematically as a tool for studying unstable nuclei. A pioneering step was the estimation of the matter radii of exotic nuclei from interaction cross section measurements (51). Many such developments over the last decade can be found in a recent volume edited by Tanihata (52).

At first sight nucleon-knockout reactions might appear to be difficult to use, both from an experimental and a theoretical point of view. We first identify some of the features that conspire to make this method such a sensitive, accurate and hence powerful tool.

3.1 General features of knockout reactions

Consider a reaction in which fast, mass A projectiles with momentum $\vec{k}_A$ have peripheral collisions with a light nuclear target and the mass $(A-1)$ residues are detected. If all light fragments remain unobserved an energy balance is not possible, but the energy of the final state of the residue can be identified by measuring coincidences with its in-flight decay gamma-rays. In the sudden approximation the momentum $\vec{k}_3$ of the struck nucleon in the projectile and that of the residue in the final state, $\vec{k}_{A-1}$, are related by

$$\vec{k}_3 = \frac{A-1}{A}\vec{k}_A - \vec{k}_{A-1}\,. \tag{5}$$

It is most convenient in experiments to consider cross section distributions with respect to a single directional component of the measured momentum. Early work on halos (53) measured the residue distributions as a function of their momentum component transverse to the beam direction. Narrow distributions were

observed, associated with the large spatial extent of the neutron halo. In fact the distributions with momentum component parallel to the incident beam are now preferred as these are much less affected by Coulomb deflection and diffractive scattering mechanisms, which are both principally transverse for forward focused reactions. This, however, requires a higher resolution. To estimate this, consider the physical parameters for the example of an incident radioactive beam of mass A=30 with energy of 80 MeV/nucleon and an exit momentum of around 10 GeV/c. The momentum width (full width at half maximum in one dimension) involved in the creation of a single-particle hole is of order 50–300 MeV/c, the lower limit being typical of a halo state, in which case a resolution considerably better than 0.5% is called for. The severity of this requirement is clear when it is remembered that the momentum spread of the incident (secondary) beam is much larger, up to 3%, for a beam from a modern fragment separator.

It was shown by Orr et al. (54), in an experiment on ^{11}Li, that this can be achieved by operating a spectrograph made of several elements in a dispersion-matched mode. In this mode the target is located at an intermediate dispersive image plane. The dispersion is then compensated in a second magnetic analyzer, so that the momentum change rather than the absolute momentum is recorded. If, for a neutron removal reaction, the field of the second analyzer is reduced by the mass ratio $(A-1)/A$, the spectrometer directly records the distribution, with respect to the quantity k_{3z} of Eq. (5), around the central residue momentum. It is instructive to compare this situation with Eq. (4) describing the (p,2p) reaction. There the quantity of interest, often called the "missing momentum", emerges as a combination of three measured momenta, whereas the energy-loss method observes this directly in spite of the poor quality of the secondary fragmentation

beam. The close analogy, also with the (e,e′p) reaction, justifies the use of the label "knockout reaction" for all three, see (24).

Much of the work cited in the following has been carried with MSU's A1900-S800 spectrometer combination (55). With the incident momentum spread limited to 0.5% it is possible to achieve a relative momentum resolution of 0.025%. Furthermore, the high beam energy, 2.4 GeV in the example given above, implies a strong forward focusing so that all reaction residues emerge within a few degrees of the beam direction, well within the angular acceptance of the spectrograph. Essentially all reactions are observed and the tracking of each individual ion through the spectrometer gives clean and background-free signals. Finally, the coincident detection of in-flight photons emitted from the residues can, after the appropriate Doppler corrections, be used to identify individual final states in the residue and provide partial cross sections and associated residue momentum distributions. (Gamma rays from other sources are revealed by their lack of Doppler shifts.) In the following momentum distributions will be compared with the theoretical calculations on a relative scale, so that only shapes and widths are compared. These identify the angular-momentum assignments in complete analogy with the angular distributions used in the classical low-energy transfer reactions. The absolute scale, expressed as the partial cross section, is then used for extracting an experimental spectroscopic factor relating the structure of the initial and final states.

The high beam momentum makes it possible to use a semi-classical theoretical description of the reaction in terms of the impact parameter of the relative motion of projectile and target. For the reactions with light targets discussed in this article, the nucleon knockout cross section to a given final state of the

residue consists of two contributions. The first component, called stripping or inelastic breakup, accounts for all events in which the removed nucleon reacts with and excites the target from its ground state. The second component, called diffractive or elastic breakup, describes the dissociation of the nucleon from the residue through their two-body interactions with the target, each being at most elastically scattered. These events result in the removed nucleon being present in the forward beam with essentially the beam velocity, the target remaining in its ground state. These processes lead to different final states, are incoherent, and their cross sections must be added in measurements where only the residue is observed. For the light targets of interest here elastic breakup due to the Coulomb interactions, called Coulomb dissociation, is small but is included for precise comparisons. The single-particle cross section can therefore be written

$$\sigma_{sp} = \sigma_{str} + \sigma_{dif} + \sigma_C \ , \tag{6}$$

where interference between the last two terms has been neglected. Except in the case of halo systems, stripping is usually the dominant nucleon removal mechanism. We will not discuss calculations of σ_C.

The stripping and diffractive cross sections are calculated using eikonal or Glauber theory (56) which has been applied extensively for the interpretation of experiments with radioactive beams (57, 58). The effects of the interactions of the removed nucleon and residue with the target enter the formalism through their phase shifts which are calculated assuming the fragments each follow a linear trajectory. The treatment of the nucleon+residue+target system is non-perturbative and contains the effects of projectile breakup to all orders.

¿From a theoretical point of view there is considerable simplification in the use of reactions on a light absorptive target such as ^{9}Be. First, it ensures that the

reaction is dominated by the strong interaction and avoids the need for a rigorous simultaneous treatment of both the Coulomb and nuclear excitation mechanisms. Second, the requirement that the residue survives the collision with the target, combined with the highly absorptive character of the residue-target interaction, ensures that nucleon removal must take place from very peripheral projectile impact parameters, leading to strong spatial localization of the reaction at the nuclear surface. The use of ^{9}Be, with no bound excited states, is an especially good choice since it presents a highly absorptive disk to the incident projectile. The surface dominance is similar but, due to the strong ion-ion absorption, is more complete than is calculated in low-energy transfer reactions where the light-ion mean free paths then determine the surface localization. The early interest in knockout reactions with radioactive beams was motivated by studies of nuclear halo states, which we now discuss.

3.2 Nuclear halo states

Single-particle motion in nuclei is rarely as simple as the extreme single-particle shell model would suggest. As discussed in Section 1, correlations of different physical origin will conspire to make the description of most nuclear states a complicated matter. The nuclear halo states encountered near the drip lines are to some extent an exception, bringing to mind the hydrogen and helium atoms of atomic physics. Nuclear halos owe their properties to the weak binding of the last nucleon (or nucleon pair), which engenders a wave function with an external tail which extends far outside of the nuclear core – the result of quantum mechanical barrier penetration. Much work has been dedicated to the halo phenomenon since it were first observed (51) and interpreted (59), e.g. the reviews (14, 60, 61) and

several papers in (62). Examples of single-neutron halos are the ground states of the deuteron, ^{11}Be, ^{14}B, ^{15}C, and ^{19}C. For a neutron halo it is usually necessary to evaluate radial integrals out to very large distances (40-100 fm). Halos with two neutrons depend upon the n-n interaction for their stability, the best two-neutron halo cases so far being ^{6}He, ^{11}Li, and ^{14}Be. Proton halos are less pronounced because of the Coulomb barrier. Good examples are the ℓ=1 proton orbital of ^{8}B, well known for its role in the solar neutrino problem, and the ℓ=0 excited level at 495 keV in ^{17}F. Proton halos with ℓ=0 are not encountered as ground states until one reaches the light phosphorus isotopes (7, 63), where the $1s_{1/2}$ state fills following the Z=14 proton sub-shell closure. Here, however, the Coulomb barrier is already sufficiently high that the tails of the halo wave functions are not very pronounced.

It was the one-nucleon removal reaction experiments on halo states which helped to develop the techniques and the understanding that have now led to the more general application of this method, to be discussed in subsections 3.3 and 3.4. Some results are given here; a more detailed discussion, including also the process of Coulomb dissociation, can be found in (14). Early, inclusive measurements of the momentum distribution of residues from halo breakup showed narrow distributions that, from the uncertainty principle, are expected to be associated with the large spatial extent of the halos. An obstacle to the understanding of halos was the theoretical prejudice that these distributions would simply reflect the square of the Fourier transform of the halo wave function. A closer analysis (64–66) shows that the measurement, in fact, samples the momentum content of the single-particle wave function $\psi_{\ell m}$ only at the nuclear surface and beyond, as was discussed above. A second obstacle was that, in all the mea-

surements on single-neutron halo nuclei, a considerable fraction of the measured cross sections actually populated excited states of the residue. This implied that the observed inclusive momentum distribution contained broad components superimposed on the narrow distribution associated with the halo state. In the last few years it has become possible to use gamma-ray coincidences to separate the individual final state components. Examples of data obtained in this way are the reactions ^{9}Be(^{15}C,^{14}C+γ)X (16) shown in Fig. 2, and ^{9}Be(^{27}P,^{26}Si+γ)X and ^{9}Be(^{19}C,^{18}C+γ)X (7) shown in Fig. 3.

The use of gamma-ray coincidences for establishing partial cross sections requires an input-output balance of the gamma-ray intensities. This may fail in more complex decays with many weak and unobserved transitions, see the discussion (67) of the decay of "Pandemonium". Experiments will show how serious this problem will be; fortunately it will be small for nuclei at the drip lines, which have very few bound states.

The high-statistics data set obtained in the reaction of ^{15}C, with a $1s_{1/2}$ ground state, clearly identifies an ℓ=0 knockout to the ^{14}C ground state and an ℓ=1 knockout to the particle hole state at 6.09 MeV. Fig. 2b also shows that the differential cross section deviates from eikonal theory, an effect that was also observed in the knockout from ^{11}Be (9). Later, in subsection 3.5, we discuss the reason for the discrepancy, which apparently is specific to halo states.

In cases where the statistics are too low to permit a detailed analysis of the gamma spectrum, it is still possible to use gamma coincidences as a tag to separate coincident and non-coincident events (7,12). This works well for ground-state halos where the subtraction of the coincident events reveals the narrow ℓ=0 momentum distributions for the ground-state knockout, as is demonstrated in Fig. 3.

For the case of ^{27}P, in (a), the dashed line marked "All wf" shows the parallel momentum distribution computed from the Fourier transform of the full radial wave function. The shoulders on this distribution are the high-momentum components due to the inner lobe of the $1s_{1/2}$ wave function. This inner region is not sampled in the reaction and the shoulders are absent from the calculation with the correct surface localization. The s-wave cross section to the ground state is 22(8) mb, only 30% of the inclusive value, and translates into a spectroscopic factor of 0.44(16) in good agreement with a theoretical value of 0.46. We see that ^{27}P is a complex-structure $1/2^+$ state, far from a clean halo structure.

The example of ^{19}C in Fig. 3 (b) demonstrates the extreme sensitivity of the high-energy knockout method. The narrow momentum distribution identifies the ^{19}C ground state as $1s_{1/2}$; a d assignment would have given a much broader distribution (dashed line). This experiment was carried out with an incident beam with less than 1 atom of ^{19}C per second (12). In spite of this, the experiment furnishes a spin assignment, a rough estimate of the neutron separation energy (0.8 MeV) and also limits on the spectroscopic factor $S_{1/2}$=0.5–1.

We now outline briefly the eikonal calculation of the momentum distributions of Figs. 1, 2, and 3. The results for the stripping mechanism show very little sensitivity to the details of the absorptive residue- and nucleon-target interactions, so it is possible to simply represent their elastic S-matrices by the strong absorption or "black disk" limit. For two-bodies the eikonal approximation (68) leaves the wave function unchanged throughout space, except that it now vanishes within a cylinder with the effective absorption radius. The model is thus geometric with the physical parameter, the black-disc radius, entering through the integration limit. In the case of a composite projectile there are two parame-

ters, the effective target radius R_T and the minimum impact parameter b_{min} for a given projectile impact parameter b. These are chosen to reproduce the empirical nucleon- and residue-target cross sections at the energy of interest. The results can be expressed (65) using cylindrical coordinates, in terms of a one-dimensional Wigner transform over the entire z axis, chosen in the beam direction. Explicitly,

$$\frac{\mathrm{dW}_{\ell \mathrm{m}}}{\mathrm{dk_z}} = \frac{1}{2\pi} \int\int\int \psi^*_{\ell m}(\vec{r}_\perp, z')\psi_{\ell m}(\vec{r}_\perp, z) e^{ik_z(z-z')} \mathrm{d}\vec{\mathrm{r}}_\perp \mathrm{dz dz'} \,, \tag{7}$$

where the integration limits are defined in terms of the vector components in the $x-y$ plane and where $\mid \vec{r}_\perp - \vec{b} \mid \leq R_T$. As is usual, the cross section involves an integral over projectile impact parameters and sums and averages over all final and initial states, respectively,

$$\frac{\mathrm{d}\sigma}{\mathrm{dk_z}} = \frac{1}{2\ell+1} \sum_m \int_{b_{min}}^{\infty} \frac{\mathrm{dW}_{\ell \mathrm{m}}}{\mathrm{dk_z}} \mathrm{d}\vec{\mathrm{b}} \,. \tag{8}$$

This procedure estimates the momentum distribution for stripping. It is assumed that the distribution for the diffractive mechanism has the same shape. We shall return to this point in Section 3.5.

In these expressions the terms with the maximum value of m are the most important, as can be seen from simple geometrical considerations. Examples of this are given in Figs. 4 and 12. This is important for the appearance of possible alignment effects in the cross sections, a subject that we take up in Section 5. Most of the momentum distributions shown in the present article have been calculated using equations (7) and (8). These approximate (black-disk) expressions also give quite good absolute stripping cross sections, typically within 20–30% of those computed using the more precise formulas to be discussed in subsection 3.3

It is also possible in special cases to derive analytical expressions for the dis-

tribution, Eq. (7), assuming the single particle wave functions are sufficiently accurately represented by their asymptotic form. For an ℓ=0 neutron halo state this is a Yukawa wave function defined by the parameter $\kappa = (2\mu S_n)^{1/2}/\hbar$, expressed in terms of the reduced mass and the neutron separation energy. For a target with a large radius, approximated by a planar cutoff, the distribution is (60, 64)

$$\frac{\mathrm{dW_{00}}}{\mathrm{dx}} = \frac{\Gamma}{2\pi}\frac{1}{(1+x^2)}\,C_1(w)\,, \tag{9}$$

where the dimensionless x is the momentum k_z in the beam direction measured in units of κ. The expression has the appealing form of the one-dimensional Wigner transform of the entire wave function multiplied by a correction function that can be expressed as a parametric integral

$$C_1(w) = \int_0^{\pi/2} \cos\theta \exp[-2w/\cos\theta]\,\mathrm{d}\theta\,, \tag{10}$$

with $w = (b - R_T)\kappa(1+x^2)^{1/2}$. The effect of $C_1(w)$ is to suppress the unphysical high-momentum components of the one-dimensional Lorentzian which arise from the singularity of the Yukawa function at the origin. The result shows that the momentum distribution should scale with the dimensionless parameter x. The comparison of the measured momentum distributions for ^{11}Be and ^{15}C is shown in Fig. 6 of subsection 3.5 and reveals that this scaling holds empirically with great precision.

It is also possible to derive analytic expressions valid in the limit of a very small target radius (65). For $\ell = 0$ the two approximations give very similar results, agree with experiments on halo nuclei, and also with the more realistic calculations based on Eq. (7). Expressions for ℓ=1 and 2 have also been derived (65, 69) but are of limited value as the use of the asymptotic form is a poor approximation to the actual wave function for non-halo states.

The halo states are, by definition, very close to a continuum threshold and the radial wave function of the least bound nucleon is very sensitive to the actual separation energy. In reactions in which a halo particle is present both before (ψ_1) and after (ψ_2) the reaction it will be necessary to consider the (radial) mismatch between the initial and final nucleon states due to the change in the average potential. Such a mismatch factor is defined as

$$M = \left| \int d\vec{r}\, \psi_2^*(\vec{r}) \psi_1(\vec{r}) \right|^2 \approx \frac{4\sqrt{S_{n1} S_{n2}}}{(\sqrt{S_{n1}} + \sqrt{S_{n2}})^2}, \tag{11}$$

where the right-hand approximation, giving the explicit dependence on neutron separation energies, is based on Yukawa wave functions and hence is appropriate only for s-states. The quantity M may be viewed as a small correction to our spectroscopic factors, which are obtained from a shell-model description that does not include continuum states. In most cases M is unity, but the correction can be of some importance if the nucleon orbital in the initial or final state is close in energy to a particle threshold. An example of this effect is provided in the (^{12}Be,^{11}Be) single-neutron knockout (10), to be discussed as an example in subsection 3.4. In this case, part of the cross section will be to continuum states above the threshold. There is a clear analogy here to the shake-off effects in atomic physics and to the "ghost states" of nuclear physics; see comments in (14).

3.3 Single-particle cross sections in eikonal theory

To provide a more accurate evaluation of the single-particle cross sections arising from the stripping and diffractive breakup mechanisms we make use of the spectator-core approximation to the many-body eikonal theory. Here core is synonymous with residue, the state of the $A-1$ nucleons following single nucleon

removal. Such an approach uses more realistic nucleon- and residue-target elastic S-matrices than the simple black-disk approximation of Eq. (7). This is essential for a quantitative discussion of deduced spectroscopic factors.

A quite general formal derivation of the inelastic breakup (stripping) cross section is presented by Hussein and McVoy (70), and is also expressed there in the spectator, eikonal limit. The essential step is that the many-body projectile-target system can be reduced to an effective three-body problem, comprising the target, residue and the removed nucleon, by use of the spectator approximation – that the $A-1$-body residue is at most elastically scattered by the target. In the absence of dynamical excitation its S-matrix with the target is diagonal with respect to core states. The removed nucleon's structure then enters the calculation through the single particle overlap function ψ_j for the specific A-body initial and $(A-1)$-body final states, discussed in subsection 2.1. Using the notation developed earlier, the stripping cross section can then be written (8, 12, 13, 71)

$$\sigma_{str} = \frac{1}{2j+1} \int d\vec{b} \sum_m \langle \psi_{jm} | (1 - |\mathcal{S}_n|^2) |\mathcal{S}_c|^2 | \psi_{jm} \rangle \, . \qquad (12)$$

The quantities $\mathcal{S}_c$ and $\mathcal{S}_n$ are the elastic S-matrices, or profile functions (72, 73), for the residue-target and removed nucleon-target systems, and are expressed as functions of their individual impact parameters with the target. These can be calculated from empirical potentials, folding approaches or multiple scattering theory. In the analyses presented, these are calculated using the optical limit of Glauber's eikonal (multiple scattering) theory (56). The nucleon-residue relative motion wave functions $|\psi_{jm}\rangle$ are calculated as eigenstates of an effective two-body Hamiltonian containing a local potential whose depth is adjusted to reproduce the physical separation energy of the nucleon from the initial state, with given

$n\ell j$, to the residue state of interest. Many calculations have been carried out assuming a fixed Woods-Saxon potential with radius and diffuseness parameters of 1.25 and 0.7 fm. In Sect. 4 the sensitivity to the choice of these parameters will be discussed. Equation (12) has a simple interpretation. It is the integral over all impact parameters, and average over m sub-states, of the joint probability of the residue scattering elastically (given by the quantity $|\mathcal{S}_c|^2$) and of the nucleon exciting the target and being absorbed from the elastic channel (given by the quantity $(1-|\mathcal{S}_n|^2)$).

The form of the corresponding single-particle cross section for diffractive breakup is less intuitive. The diffractive cross section, summed over all continuum relative motion final states of the nucleon-residue system (13), is

$$\sigma_{dif} = \frac{1}{2j+1}\sum_{\sigma,m}\int d\vec{k}\int d\vec{b}|\langle\psi_{\vec{k}\sigma}|(1-\mathcal{S})|\psi_{jm}\rangle|^2\,, \tag{13}$$

where we have abbreviated $\mathcal{S}=\mathcal{S}_c\mathcal{S}_n$. Here, consistent with the spectator core approximation, the continuum breakup states $\psi_{\vec{k}}$ are assumed eigenstates of the same two-body Hamiltonian which initially bound the pair. Completeness of the bound and continuum two-body eigenstates then gives, using closure,

$$\sigma_{dif} = \frac{1}{2j+1}\int d\vec{b}\sum_{m,m'}\left[\langle\psi_{jm}|\,|1-\mathcal{S}|^2|\psi_{jm}\rangle\delta_{mm'} - |\langle\psi_{jm'}|(1-\mathcal{S})|\psi_{jm}\rangle|^2\right]\,, \tag{14}$$

eliminating the need to carry out integration over the continuum. In writing Eq. (14) we have also assumed that the spectrum of the two-body Hamiltonian has only a single bound state ψ_j. While clearly an excellent approximation for light halo states, where the ground state is often the only bound state, in general, other bound states will contribute additional terms that must also be subtracted on the right of Eq. (14). These off-diagonal bound state matrix elements take the form

of single-particle inelastic excitations that are very small (13) at intermediate energies. Their effect will be to reduce the diffractive cross section calculated using Eq. (14).

Reactions in which a weakly bound valence nucleon is present both before and after the reaction, but with significantly different separation energies, were discussed in the preceding subsection in connection with the radial mismatch factors. An additional consideration is in transitions where a more bound nucleon is stripped from a halo nucleus, or one with weakly bound valence nucleons. Such situations arise in the stripping of $p_{3/2}$ and $p_{1/2}$ neutrons from the $1/2^+$ ^{11}Be and ^{15}C ground states, respectively. The reaction residue (core) in such instances is itself a weakly bound composite (8), with an enhanced absorption and reduced survival probability, due to the breakup mechanism with the target. In such cases the residue should therefore be treated as a composite, of a mass $A-2$ core b and a nucleon bound in a state ϕ, and the residue-target S-matrix $\mathcal{S}_c$ calculated according to (8)

$$\mathcal{S}_c = \langle \phi | \mathcal{S}_b \mathcal{S}_n | \phi \rangle \, . \tag{15}$$

For neutron halo states, Eqs. (12) and (14) make roughly equal contributions to the single-particle cross section. This is related to the early finding that the total cross section for fast neutrons is approximately twice the geometrical value. An experiment with ^{11}Be, incident at 41 MeV/nucleon on a ^{9}Be target (74), observed the broad angular distribution of the neutrons (out to 20 degrees) expected from the diffractive process. The measured cross section of 120(24) mb was close to half of the inclusive cross section of 290(40) mb, as expected for a pronounced halo state incident on a strongly absorptive target. A new experiment at the GSI (75) has determined an elastic-breakup cross section of 26.9(1.4) for

^{11}Be at 520 MeV/nucleon on a carbon target. This is in good agreement with theoretical values of 28–32 mb, depending on the particular choice of parameters. (According to theory 17% of the cross section is from Coulomb breakup.) For more strongly bound states the contribution from stripping, Eq. (12), is typically a factor of 2–3 greater than that from diffraction, Eq. (14). There is actually very little experimental evidence of the two individual contributions. A recent experiment by Enders et al. (18) was able to test the ratio in the case of proton knockout. For ^{8}B, with the results summed over the two populated ^{7}Be final states, they found values of 1.8 (theory) and 2.5(9) (experiment) for the stripping-to-diffraction ratio. The corresponding results for ^{9}C were 2.2 (theory) and 2.8(9) (experiment). In both instances the results agree within the experimental errors, but there is perhaps an indication that the diffractive breakup is relatively weaker than predicted by theory.

The essential parameters used in the calculation of the S-matrices $\mathcal{S}$ are an effective nucleon-nucleon interaction and the assumed matter distributions, and their root mean squared (rms) radii, of the core and target nuclei. The effective interactions are constructed using the empirical free nucleon-nucleon cross sections (76) and the theoretical real-to-imaginary part ratios of the forward scattering nucleon-nucleon amplitudes, as tabulated by Ray (77) for intermediate energies. The effective interaction was assumed to be of zero-range for energies above 0.3 GeV/nucleon. For all lower energies a Gaussian form, of range 0.5 fm, was used (8) which reproduces measured ion-ion reaction cross sections for systems such as ^{12}C – ^{12}C and ^{27}Al – ^{12}C at 83 MeV/nucleon (78), and the proton–^{9}Be system at 60 MeV/nucleon (79). The point-particle rms matter radii for many of the reaction residues of interest are now available as measured values; see the review

by Ozawa et al. (80). Our results are rather insensitive however to fine details of the assumed matter radii.

3.4 Examples of spectroscopy with knockout reactions

There is accumulating evidence that in neutron-rich nuclei near the drip line the conventional shell gaps associated with the magic numbers disappear and that new gaps corresponding to other subshell combinations appear. As a clear example, in Table 1 we show the case of the N=8 nucleus ^{12}Be studied in the ^{9}Be(^{12}Be,^{11}Be+γ)X neutron knockout reaction (10). The reaction populates the $1s_{1/2}$ ground state and the $0p_{1/2}$ excited state of ^{11}Be at 320 keV, the latter being the only bound excited state in this nucleus. A closed p-shell for ^{12}Be would imply a spectroscopic factor close to 2 for this $1/2^-$ excited level at 320 keV. The gamma spectrum in coincidence with the ^{11}Be residues does reveal a strong gamma-ray of this energy, but the corresponding intensity and absolute cross section is only one quarter of that expected for the closed shell. Furthermore, the cross section to the $1/2^+$ ^{11}Be ground state is twice as large revealing the presence of an important $[1s_{1/2}]^2$ component in the ^{12}Be wave function, and showing that the *sd*-shell has already begun to fill appreciably at N=8. The measured residue momentum distributions associated with the two states confirm the expected ℓ=0 and 1 assignments.

The quantitative details shown in the Table have been expanded somewhat from the original publication (10) to illustrate more details of the analysis of a knockout experiment. The nuclear single-particle cross sections have been calculated from Eqs. 12 and 14. The initial state in this case consists of a pair of valence nucleons, one of which is a spectator, and the final state residues are

halo nuclei. This is a case where the few-body composite structure of the residue must be taken into account and the $\mathcal{S}_c$ corrected, according to Eq. (15). This correction is small in the case of ^{12}Be, compared to the 10-15% reduction of the single particle cross sections obtained for the removal of $p_{3/2}$ core-state neutrons from ^{11}Be (8,9). Relative to a one-body core calculation, based on an rms matter radius of 2.45 fm (the average of the measured values for ^{10}Be and ^{12}Be (80)) the composite-core cross section is lower by about 2% for the s-state and higher by about the same amount for the two other states.

For completeness the Table also includes the single-particle Coulomb dissociation cross section σ_C (81), which turns out to be negligible. The large difference in neutron separation energies between ^{12}Be and ^{11}Be means that the mismatch factors M, calculated from Eq. (11), differ appreciably from unity. The experimental spectroscopic factors are obtained by dividing the experimental cross sections by the total σ_{sp} and by the mismatch factor M. In this way the results can be compared directly with those theoretical spectroscopic factors (10, 82) which include the center-of-mass correction, which they did not in (10).

The spectroscopic factors to the two final states are both close to 0.5, well below the sum rule total of 2. The missing components are almost certainly in the $[0d_{5/2}]^2$ configuration, however knockout from this component will lead to the unbound $0d_{5/2}$ configuration in ^{11}Be and therefore cannot be observed in a gamma-ray experiment. This experiment is a direct demonstration of the breakdown of the N=8 shell closure and shows a pairing-type wave function with comparable $[1s]^2 + [0p]^2 + [0d]^2$ components, characteristic of a deformed nucleus. This is especially striking because the even-even ^{14}C neighbor, with 8 neutrons, is very magic. (We note for completeness that the fact that the $1s_{1/2}$ intruder is

the ground state in ^{11}Be does not permit simple conclusions about ^{12}Be; the measurement shows that the ground state is very different from $[1s_{1/2}]^2$.) The highly deformed character of ^{12}Be finds support in two recent experiments by Iwasaki *et al.* (83). Using inelastic scattering on a proton target they find evidence for a strong quadrupole deformation of the neutrons and, upon a heavy target, a strong E1 excitation to a 1^- level at only 2.68 MeV. The ^{12}Be experiment also poses the question; Does the neutron halo of the N=8 neighbor, ^{11}Li, also have a significant $0d_{5/2}$ neutron component? This was not considered in the recent experiment on continuum states and which will be discussed in subsection 3.6.

Other examples are provided by the nuclides ^{15,17}C, shown in Figs. 2 and 1. Detailed discussions can be found in the original papers (12, 16), which demonstrate the potential of the knockout method for testing both spin assignments and, through the spectroscopic factors, details of the composition of the many-body wave function. The identification and interpretation of the mixed ℓ=0,2 transition, shown in Fig. 1 (b), is a particularly striking example. Although single-nucleon Coulomb dissociation is outside the scope of the present article, it is instructive to compare the knockout analyses with recent GSI results (84), which studied the same two nuclei using reactions on a lead target. The results clearly demonstrate the selectivity of Coulomb dissociation to *s*- and halo-state components, for which it complements knockout reactions in an interesting way. Coulomb dissociation is likely to be of only limited value for deeply bound or higher ℓ states.

An example of a proton halo state is provided by ^{8}B, where the proton is bound by only 0.1375 MeV. We will return to this nucleus in the later subsection 4.1, in connection with the determination of absolute spectroscopic factors from

knockout reactions. The nucleus ^{8}B has been the subject of numerous studies because of its importance for the solar neutrino problem. A recent GSI experiment by Cortina-Gil et al. (85) has measured gamma-rays in coincidence with ^{7}Be residues and obtained their inclusive and exclusive parallel-momentum distributions. The data are shown in Fig. 4 and are in good agreement with calculations based on Eqs. (7) and (8). An alternative analysis, based on eikonal reaction theory and a cluster model, are presented in (85) and give very similar results. The dashed lines show the relative contributions of the $|m|$=0 and 1 proton magnetic sub-states to the inclusive spectrum. We note that the contribution from the $|m|$=1 components is greater by more than the factor of 2 expected from statistical weights, suggesting a general possibility of alignment effects. This will be discussed briefly in subsection 5.2.

As a final example, in Fig. 5 we show residue momentum distributions for the one-neutron knockout on ^{34}Si, which has 20 neutrons. The experiment finds cross section to only three final states (15), the ground state ($\frac{3}{2}^{+}$), a state at 1.01 MeV ($\frac{1}{2}^{+}$), and a state at 4.49 MeV ($\frac{5}{2}^{+}$) corresponding to the three *sd*-shell orbitals. The assignments are clear, although the difference in shapes for the two ℓ values is far less pronounced than for the halo cases of Figs. 2b and 3b, because of the relatively high neutron separation energy, 7.54 MeV, of ^{34}Si. (The analogous effect is well known for transfer reactions where the angular distributions are less distinct for deeply bound states.) The spectroscopic factors S_j of the lowest two states are close to the maximum sum-rule values, $(2j + 1)$; represented by the two points on the extreme right on Fig. 5b. This shows that the shell closure at N=20 is preserved in ^{34}Si; this is interesting since it is known that the shell gap breaks down for ^{32}Mg with just two protons less. Knockout studies on this and

other cases in this mass region are possible and can serve to map how negative parity intruder states affect the structure as the drip line is approached.

The data in Fig. 5a also invite a first discussion of the, largely unanswered, question of the absolute velocities of the residues which, in the sudden approximation, are equal to those of the projectile. This is the no momentum transfer assumption underlying Eq. (4). The (nominal) beam momentum of the ^{34}Si experiment was calculated to be 12.270(30) GeV/c in good agreement with the observed peak values for the $3/2^+$, $1/2^+$, and $5/2^+$ states of 12.200(4), 12.250(3), and 12.250(10), respectively, where the errors are statistical only. The fact that the experimental distributions were measured at one setting of the spectrograph, and represent subsets sorted on the basis of coincidences with γ-rays, permits a more accurate statement about relative momenta since the absolute scale drops out. The distribution associated with the $3/2^+$ ground state is centered at a parallel momentum that is lower than those of the two higher levels by 50(5) MeV/c. A similar effect can be seen in the ^{15}C data of Fig. 2b, except that in this case it is the excited level that is shifted down by approximately 8 MeV/c relative to the ground state. The origin of these (small) shifts remains an interesting puzzle. That shifts of opposite sign are obtained for two excited states would seem to rule out a simple connection to energy and momentum conservation laws.

Finally, we compile and examine how well the spectroscopic factors deduced from the 27 partial cross sections measured so far by the γ-coincidence method agree with structure theory for the $p-sd$ shells. Fig. 5b shows that the results, expressed in units of the maximum sum-rule value $(2j+1)$, agree very well. The four points which are lower than the systematics correspond to states at excitation energies of 6 MeV (in ^{10}Be and ^{14}C), and at 4.3 MeV (in ^{33}Si). It is possible

that they indicate that at these separation energies the single-particle strength is spread more, or differently, than given by theory. Alternatively the reduction factor, R_s, of roughly a factor of two, could reflect a quenching of shell-model strength associated with short-range correlations, which we discuss in subsection 4.1. The consistency and accuracy of the combination of the shell model and eikonal reaction theory also finds support in a series of measurements of inclusive cross sections for 22 nuclides in the Z=5–9 region carried out by Sauvan et al. (86). In the absence of γ-coincidences and partial cross sections it is necessary to compare the measured cross sections with the sum of all theoretical knockout partial cross sections below the neutron threshold. The results translate into a weighted experiment-to-theory ratio average of 0.92 ± 0.04, see (14), in good agreement with the results of Fig. 5b.

3.5 Non-eikonal theoretical models

Two approximations underpin the eikonal few-body model description of the stripping and diffractive breakup mechanisms discussed in subsection 3.3 and exploited above. The first is the adiabatic or sudden approximation – that the projectile energy is sufficiently high, and hence the collision time sufficiently short, that the residue-removed nucleon relative motion can be considered frozen during the collision. The approximation is implicit in our Eqs. (12) and (14) where the reaction S-matrices are calculated at fixed impact parameters and then appropriately averaged over all available configurations of the constituents in the projectile. Formally, the approximation to the full three-body model is that, for the purpose of the reaction dynamics, the excitation energy associated the relative motion of the nucleon and residue is small and is neglected (87).

The approximation does not conserve energy and, in particular, does not account for energy transfer between the center-of-mass and relative-motion degrees of freedom of the residue and removed nucleon. The adiabatic condition is well satisfied for collisions on a light target at intermediate energies.

The second, eikonal, approximation is that, having made the adiabatic approximation, the Schrödinger equation can be solved assuming the projectile's constituents follow (constant velocity) straight-line paths. It is assumed, therefore, that the elastic S-matrices entering Eqs. (12) and (14) are computed accurately in this limit (56). Calculation schemes which remove one or both of these approximations are available to assess their importance.

One such recent study has been carried out by Esbensen and Bertsch (88), using direct numerical solution of the time-dependent Schrödinger equation to assess the eikonal few-body approach. The time-dependent approach follows the evolution of the nucleon's wave function in the time-dependent potential field it experiences with the target (89). The approach thus does not involve either adiabatic or eikonal approximations for the nucleon motion. On the other hand, the heavy residue's motion is still assumed to follow a simple trajectory with constant velocity and so is not treated dynamically, and cannot share energy with the target and nucleon. The analysis shows that the eikonal approximation underestimates slightly the calculated single particle cross section at all energies, but with a maximum deviation of only 20% at the lowest energy considered, 20 MeV/nucleon. At the energies of the knockout reaction analyses considered here, the deviation is at most a few percent (88). These reduced cross sections of the eikonal model are simply understood, since the eikonal nucleon-target S-matrices calculated from potential models have a smaller spatial extent (90),

effectively underestimate the size of the target, and underestimate the nucleon-target reaction cross section at low energies. Given the surface dominance of the knockout reaction both the stripping and diffractive cross section contributions are also reduced. Calculations which use an exact nucleon S-matrix, obtained by analytically continuing the partial wave S-matrix, and which calculates the correct reaction cross section, are qualitatively and quantitatively very close (91) to the non-eikonal calculations of Ref. (88).

A closely related treatment of the reaction is provided by the transfer-to-the-continuum (TC) approach of Bonaccorso and Brink (92), developed from the semi-classical transfer model of Hasan and Brink (93). Once again the nucleon's motion is allowed to evolve with time, and the adiabatic and eikonal approximations are not made. In addition, by assuming the residue follows a straight line path, and that the final state interactions of the nucleon and the residue can be neglected, the need for a time-dependent solution is avoided and much of the calculation can be carried out analytically. However, an important additional approximation required to enable the analytic reduction, is that only the (Hankel function) asymptotic form of the nucleon-core initial bound state and (S-matrix) of the nucleon-target final state wave function are involved. While this will be a reasonable approximation for the neutron halo states, this approximation is not quantitative for more bound and non-s-state transitions, as was discussed in the context of the analytic formulae for the momentum distributions in subsection 3.2. Nevertheless, an interesting prediction of this model is that for $\ell = 2$ transitions, the linear and angular momentum matching conditions involved in the nucleon's transfer between the residue and the target lead to momentum distributions with a marked asymmetry (94). This prediction has yet to be confirmed

experimentally with data of sufficient statistics. In cases where the eikonal and TC model predictions for the σ_{sp} have been compared directly, e.g. (15, 95), the agreement is very good.

Very recently (16), the coupled discretized continuum channels (CDCC) method (28, 29) has also been used to investigate the accuracy of the eikonal method. The CDCC proceeds by constructing a square integrable basis of relative motion states in the separation of the projectile constituents on which to expand the three-body wave function of the projectile and target. Using this basis, the CDCC approximates the three-body problem by an effective two-body coupled channels equation set. Unlike the methods discussed above, the CDCC solves the full three-body problem without approximation of the three-body dynamics. To date, the CDCC has been used to calculate only the diffractive breakup part of the knockout reaction. The calculations, see Table I of (16), confirm that the integrated diffractive single particle cross sections of the eikonal model are reliable. The CDCC also permits the study of more precise features of the data, such as the observed low momentum tail on the measured parallel momentum distributions for the ground state to ground state transitions in ^{11}Be and ^{15}C (9, 16), see also Fig. 6. By definition, the momentum distributions are symmetric, see Fig. 2, within the eikonal model.

Details of the CDCC, of the calculation of the breakup triple differential cross sections, and of the parallel momentum distributions of the residues can be found in Refs. (16,96). For breakup of the ^{11}Be and ^{15}C halo systems on a ^{9}Be target at 50-70 MeV/nucleon incident energies, breakup energies up to 30 MeV and relative motion partial waves up to g-waves were needed in the neutron-residue system. Such values are rather universal, reflecting the linear and angular momentum

transfer induced by the surface diffuseness of the constituent-target nuclear tidal interactions.

Figure 2 shows the measured momentum distributions for the ^{15}C beam of 54 MeV/nucleon. The broken curves are the eikonal calculations. The solid curve, which includes the CDCC calculation of the elastic breakup component, is seen to give an excellent description of the measured asymmetry of the ground state momentum distributions. The agreement with the ^{11}Be data is of equal quality. We attribute this agreement to our correct treatment of the continuum, of the flux excited, and of the reduction in energy available to the residues. To date this effect has been observed experimentally only for halo states, which is consistent with the large diffractive cross section component in these cases.

The details of the distributions in Figure 6(a) are now fully understood, and can be reproduced with high accuracy. This being the case, Figure 6(b) now adjusts the momentum scale for the ^{11}Be data, according to the ratio of the ^{15}C and ^{11}Be separation energies, $\sqrt{1.218/0.503}$, to test the scaling property discussed following Eq. (10). It is clear that the data sets are essentially identical upon scaling, reflecting the universal character of the distribution, including the low momentum tail, for these halo systems.

3.6 Knockout to continuum states

It is possible although much more delicate to apply direct reactions to study nuclei with no bound states. We take as a specific example the N=7 isotones, where ^{11}Be marks the neutron drip line. Here, single-particle states in the systems located one and two steps beyond the drip line, ^{9}Li+n and ^{8}He+n have both been studied in direct reactions. Especially for the *s* states, which are not expected

to show a resonant behavior, the ideal approach would be to measure the phase shifts from neutron elastic scattering as a function of energy, but, although both nuclei as well as neutrons are available as beams, none are available as a target. An alternative is to investigate final-state interactions in the decay spectra of the unbound residual nuclei (here, ^{10}Li and ^{9}He) formed in direct one- and two-proton knockout reactions from ^{11}Be (97, 98). As the valence neutron in the projectile is predominantly in an $1s_{1/2}$ state, these reactions will have a favorable spectroscopic strength to an $\ell = 0$ neutron final state. Both show a strong final-state interaction in the ℓ=0 channel indicative of a low-lying s-state. The strength of this neutron interaction is best parameterized in terms of the neutron scattering length a_s, with $|a_s|$ found to be large in both cases: For ^{9}Li+n, $a_s < -20$ fm, and for ^{8}He+n, $a_s < -10$ fm. This suggests that the $1/2^+$ virtual states are the ground states of ^{10}Li and ^{9}He. This is expected from the level systematics of the $N = 7$ isotones, based on data from (97, 99–102), see Fig. 7 and Ref. (103).

To understand the momentum distribution of the $(A-2)$ residue in the breakup of a two-neutron halo has presented a long-standing problem. Work by Simon *et al.* (104) has demonstrated how to approach this problem. They reconstructed the combined momentum of the ^{9}Li+n residue, formed in the stripping of a neutron from ^{11}Li on a light target. This relates to the momentum distribution of the stripped neutron in the same way as for the reactions to bound states discussed above. The measured momentum distribution could be resolved into approximately equal contributions from $[1s]^2$ and $[0p]^2$ components. An even more striking signature was obtained in that experiment by observing the angular correlation of the decay products from the recoiling ^{10}Li, Fig. 8. The strong forward-backward asymmetry observes directly the interference between the l=0

and 1 final states. Similar experiments have been carried out for ^{6,8}He by Markenroth et al. (105).

4 ABSOLUTE SPECTROSCOPY AND SHORT-RANGE CORRELATIONS

Very recently, work has been carried out to assess whether the one-nucleon knockout reaction is able to provide accurate absolute occupancies of orbitals in the valence shell (17,18). These initial studies suggest that this is indeed the case. If this holds as more experimental evidence becomes available, it will allow a more systematic exploration of the foundations of the shell model, incorporating data for both neutron and proton orbitals. Experimentation with radioactive beams will also allow the study of loosely bound states in very unstable systems, such as nuclear halo states.

The wider perspective is that data of this kind may reveal the contributions from correlations in the single-particle motion caused by the repulsive short-range part of the nucleon-nucleon interaction. This was the subject of the earlier discussion, in subsection 2.2, of the (e,e′p) reaction, which has been considered uniquely able to access absolute spectroscopic factors. This Section also presents the, still limited, evidence for the use of knockout reactions for determining the asymptotic normalization coefficients of single-particle wave functions, an application recently suggested by Trache et al. (106). In this connection we assess the likely precision with which spectroscopic factors and asymptotic normalization coefficients can be obtained from these surface-dominated cross sections.

4.1 Quenching factors R_s from knockout reactions

Several papers have now attempted to analyze how well measured cross sections agree with the theory outlined in Section 3. For the set of about 25 measured partial cross sections, most for weakly bound nucleons in the $p-sd$ shells, a first survey (14,15) found that a plot of the deduced experimental spectroscopic factor versus that of theory (the shell model) had a strong correlation with most but not all points close to the diagonal. However, in many cases the experimental errors are still large and the theoretical values are not expected to be very precise. It is therefore difficult to reveal the presence of significant re-scaling on the basis of such a broad data set.

A more exacting comparison has been carried out by Brown et al. (17) and Enders et al. (18) by selecting cases where the structure is well studied and well understood, such as ^{16}O, ^{12}C and also the radioactive ^{8}B and ^{9}C. For these cases accurate inclusive cross section data, good to $\approx$5%, have also been taken over a wide range of energies, for the ^{8}B case from 0.08 to 1.44 GeV/nucleon. This range tests that the spectroscopic factor is extracted consistently; furthermore the eikonal model is at its most reliable at high energies. Several refinements were made to make the analysis as accurate as possible. The rms radii of the projectile cores and the target were taken from experiment. In the earlier systematic studies (14) the wave functions describing the nucleon-core relative motion were calculated in a Woods-Saxon potential with a "standard" set of radius and diffuseness parameters r_0=1.25 fm and a=0.7 fm. For the test cases discussed here, it was possible to use optimized values based on experiment or, in the case of ^{15}C, on a self-consistent Hartree-Fock calculation. For each of the three projectiles discussed in the present work, analyses exist that permit the selection of

such an optimized set. Use of the"standard" set does not change the conclusions appreciably.

Under the assumption that the correlations arising from the long-range part of the nuclear force are included in the theoretical spectroscopic factors S_j^{th} we define an empirical reduction factor attributed to short-range correlations

$$R_s = \frac{S_j^{exp}}{S_j^{th}}\,, \tag{16}$$

for a partial cross section with a single j value. For an analysis of an inclusive knockout cross section, the average R_s can be defined as the ratio of the cross section to the sum of the theoretical cross sections to all states that lie below the nucleon threshold, see (17). As for (e,e′p) analyses, the deviation of R_s from unity provides a measure of the effect of the strong correlations at short distances.

The results of the analyses for the cases where the nucleons are strongly bound are shown in Figure 9. The effective separation energies here cover the range 10–19 MeV. The results for protons, of 0.5–0.65, are in good agreement with those from (e,e′p) reactions (46). The results for neutrons, which could not be obtained in electron scattering experiments, are very similar as would be expected from isospin symmetry. It will be seen that the physical occupancies are very much lower than those suggested by shell model calculations, which use effective interactions and neglect the effects of short-range correlations. A completely different picture emerges for the data taken with loosely bound, halo-like states, shown in Figure 10. In these cases the R_s factors are close to 0.9 and suggest that the effects of short-range correlations are much less important for weakly bound states. (This may explain why the first analyses, discussed above, find little quenching of the spectroscopic factors.) The interplay of long- and short-range correlations clearly poses an interesting challenge to theory and to

experimentation with radioactive beams in the years to come.

4.2 Experimental sensitivity to single-particle orbitals

Nuclear astrophysics studies often need absolute cross section information in an energy range that is not directly accessible to experimentation. For radiative capture reactions, an essential quantity of interest is the large-distance behavior of the bound-state wave function, while the continuum single-particle wave function is assumed to be better understood. In a recent interesting paper, Trache *et al.* (38) start from the assumption that knockout reactions furnish precise absolute occupancies, a viewpoint that finds support in the results presented in subsection (4.1). From Eqs. (2) and (3), and the definition of R_s, Eq. 16, we can obtain an expression for the asymptotic normalization coefficient

$$C_\ell^2 = \frac{\sigma_{exp}}{(\sigma_{str} + \sigma_{dif} + \sigma_C)} \left(\frac{r_L \, R_\ell(r_L)}{W_{-\eta,\, l+\frac{1}{2}}(2kr_L)} \right)^2 , \qquad (17)$$

where a possible contribution from Coulomb dissociation has been included. This expression is conveniently insensitive to specifications of nuclear-structure parameters and illustrates why the asymptotic normalization coefficient can be obtained with somewhat higher precision than the spectroscopic factor (38). The essential point is that the square of the single-particle wave function and the theoretical cross sections are correlated. We examine this question further below. The technique has been applied to deduce the asymptotic normalization of proton wave functions for the ^{8}B and ^{9}C nuclei (17, 18, 38, 106). The results are consistent with measurements by other methods.

Knockout reactions sample the nucleon wave functions near the nuclear surface. Information deduced on absolute spectroscopic factors must therefore involve an extrapolation to take account of the interior parts of the wave function. We can

estimate the fraction of the wave function observed by the ratio of the single-particle stripping cross section to the free-nucleon reaction cross section with the target. For a pronounced halo system such as the $1s_{1/2}$ neutron state of ^{11}Be, with a separation energy of 0.503 MeV, this fraction is close to 50%, while for ^{15}C, with a neutron separation of 1.218 MeV, the fraction is 30%. The $0p_{3/2}$ state of ^{8}B is only a moderate proton halo in spite of a separation energy of only 0.1375 MeV (the effect of the Coulomb barrier) with a fraction of about 25%. For a deep hole state such as the $0p_{1/2}$ neutron in ^{12}C, bound by 18.7 MeV, the fraction detectable at 250 MeV/nucleon is only 12%.

The errors arising from the implicit extrapolation can be estimated from expressions (2), (12) and (14). Evaluating their partial derivatives with respect to the Woods-Saxon potential parameters, in a finite-difference approximation, one obtains, for some of the cases above,

$$^{15}\mathrm{C}\ :\ \delta(\mathrm{S}_j)/\mathrm{S}_j = -0.40\,\delta r_0 - 0.81\,\delta a$$

$$^{8}\mathrm{B}\ :\ \delta(\mathrm{S}_j)/\mathrm{S}_j = -0.52\,\delta r_0 - 0.96\,\delta a\ ,$$

where the coefficients are given in fm^{-1}. These suggest errors of 2–10 %. Deeply bound core states are mainly sensitive to r_0, with a coefficient of the order -1.2. The values chosen for r_0 and a are normally correlated; this effect can be examined by choosing the root-mean-square radius r_{rms} and a as the independent variables. This leads to

$$^{15}\mathrm{C}\ :\ \delta(\mathrm{S}_j)/\mathrm{S}_j = -0.41\,\delta r_{rms} - 0.025\,\delta a$$

$$^{8}\mathrm{B}\ :\ \delta(\mathrm{S}_j)/\mathrm{S}_j = -0.43\,\delta r_{rms} - 0.004\,\delta a\ ,$$

which shows that, with these variables, the spectroscopic factors are independent of a and that an error of 0.1 fm on the radius leads to a 4% error on the spec-

troscopic factor. The determination of the asymptotic normalization coefficient benefits from correlated factors in the numerator and denominator to give for the case of ^{8}B

$$^8\mathrm{B}\ :\ \delta(C_\ell^2)/C_\ell^2 = 0.24\,\delta r_0 + 0.59\,\delta a\ ,$$

a factor of two more precise than the relative spectroscopic factor.

5 NEW DEVELOPMENTS

5.1 Two-nucleon knockout as a direct reaction

In a recent paper, Bazin *et al.* (114) show evidence that two-proton removal reactions from neutron-rich nuclei proceed as direct processes. The basic reason for this is that the alternative process of one-proton knockout followed by proton evaporation is strongly suppressed relative to gamma decay and neutron evaporation from the intermediate states. This is brought about by the asymmetry in proton and neutron separation energies; for the example below the proton channel from ^{27}Na only opens up above 13.3 MeV excitation energy. The technique for observing this process is basically the same as that for one-nucleon removal reactions discussed in subsection 3.4. Fig. 11 shows the momentum distribution of the residues and the coincident gamma-ray spectrum obtained for the reaction ^{9}Be(^{28}Mg,^{26}Ne)X. From the point of view of nuclear structure this is a fairly transparent example because the reaction connects two spherical *sd*-shell nuclei which are stabilized by the pronounced N=16 sub-shell closure (3).

Direct reactions involving two particles differ fundamentally from one-particle reactions. For single-nucleon knockout in the sudden approximation, discussed in Section 3, and for single nucleon transfer reactions, the theoretical cross sec-

tions often factorize as a product of a reaction dynamics and a structure term. This very convenient feature does not generalize to reactions involving two nucleons. In two-nucleon knockout (and two-particle transfer reactions) the transition amplitudes for a given total angular-momentum transfer J are now a coherent superposition of many contributing pair combinations. The transition amplitudes thus mix inextricably the dynamical and structural aspects.

As was noted by Bazin *et al.* (114), two-nucleon knockout has important differences from two-particle transfers. In the latter, the transfer vertices impose selection rules which often dictate that the nucleon pair must transfer as a spin singlet, isospin triplet combination. For the knockout reaction such selection rules do not operate and any configuration of the pair of particles in the valence shells can contribute. It is then possible to start from the assumption that the two particles are uncorrelated, except for those spatial correlations implicit through their binding to a common core. Eikonal reaction theory (8) then suggests that the basic unit of cross section, neglecting spin-orbit splitting for simplicity, is (with $\hat{\ell}^2 = 2\ell + 1$)

$$\sigma_{\ell_1\ell_2} = \frac{1}{\hat{\ell_1}^2\hat{\ell_2}^2} \sum_{m_1 m_2} \int d\vec{b} \langle \ell_1 m_1, \ell_2 m_2 | (1 - |\mathcal{S}_{p1}|^2)(1 - |\mathcal{S}_{p2}|^2)|\mathcal{S}_{\rm c}|^2 | \ell_1 m_1, \ell_2 m_2 \rangle \,, \tag{18}$$

the two-nucleon analogue of Eq. (12). The proton-residue relative motion wave functions $|\ell m\rangle$ are once again calculated in a Woods-Saxon potential whose depth is adjusted to reproduce the observed proton separation energies. The recoil of the heavy residue is neglected. Diffractive breakup processes are assumed to be negligible for the neutron rich systems with very deeply bound proton states. For two-proton removal from the *sd*-orbitals of ^{28}Mg, these elementary cross sections are $\sigma_{22} = 0.29$ mb, $\sigma_{00} = 0.35$ mb, and $\sigma_{20} = 0.32$ mb. (In addition to the

uncertainty introduced by the approximation, it should be kept in mind that for deeply bound states the absolute spectroscopic factors discussed in subsection 4.1 are reduced by approximately a factor 0.5. We may expect to encounter similar effects in the two-proton reaction.) To convert the theoretical unit cross sections into a two-nucleon knockout cross section, one needs to define the appropriate spectroscopic amplitudes. Within the extreme independent-particle approximation, it follows from simple combinatorics that for p particles in the valence shell the factor multiplying the pair cross sections is $S_p = p(p-1)/2$. For ^{28}Mg, with p=4, the calculation based on σ_{22} then gives 1.8 mb in good agreement with the measured inclusive cross section of 1.50(10) mb given in Fig. 11. This yields strong support for the direct reaction interpretation.

A second check of this interpretation comes from the shape of the parallel-momentum distribution of the residues shown in the left part of Fig. 11. The relatively narrow parallel-momentum distribution centered close to beam velocity is, qualitatively, the signature of a direct reaction. A more quantitative interpretation requires, in principle, the differential equivalent of Eq. (18). The task of calculating this may, however, be simplified by our earlier observation that this distribution probes the wave function's momentum content only in the surface of the nucleus, and that this quantity changes only slowly with the distance from the core. The distribution for two independent particles is then, to a good approximation, given by folding those for two independent nucleons. The theoretical curve in the left part of Fig. 11 was obtained in this way and lends further support to the interpretation of the reaction as a direct knockout of a two protons from the 0d orbital. Other interpretations, shown in the figure, agree less well. We expect that the shapes of two-proton momentum distributions will

be of less value as a diagnostic tool than the one-nucleon process because each J channel will mix several different ℓ values. This should make the shapes less characteristic.

The calculation of spectroscopic strength to individual final states requires a more detailed model. In their first analysis, Bazin et al. (114) assume that the four valence protons in ^{28}Mg are restricted to the $0d_{5/2}$ sub-shell. With this, the possible final states of ^{26}Ne are 0, 2, and 4^+, with spectroscopic factors 4/3, 5/3 and 3, respectively, and which sum to the inclusive value $S_p = 6$ given above. Dividing the approximate partial cross section obtained from Fig. 11 by the unit cross section σ_{22}, they obtain (in the same order) 2.4(5), 0.3(5), and 2.0(3) in semi-quantitative agreement. The low cross section to the 2^+ level presents a problem in this very simple model. If on the other hand they use shell model wave functions, and in addition restrict the two protons to a relative $0s$-state configuration, they find pronounced destructive interference in the J=2 channel, and spectroscopy in agreement with the experiment (114). This calls to mind the "fingerprints" characteristic of one- and two-nucleon transfer reactions on complex nuclei, see Ref. (115).

The reaction and its converse, the two-neutron knockout on proton-rich nuclei, are very promising tools for spectroscopy of exotic nuclei. They lead directly toward nuclei whose yield is extremely small in any production process. We expect that the cross sections will provide specific and quantitative information on nuclear structure. Furthermore, the method should be applicable over a wide mass range. We note in this context that our example, ^{28}Mg, is closer to stability (^{32}S) than it is to the drip line (^{22}C).

5.2 Alignment effects and gamma-ray angular distributions

As was mentioned in subsection 3.2, the surface character of the single-nucleon knockout reaction is reflected in the observed momentum distributions in a characteristic way, described approximately by Eq. (7). For single-particle angular momenta $j > 1/2$, the cross sections are also dependent on the individual m substates, with the possibility of a resulting alignment effect. In this sub-section we discuss some possible consequences and future applications of this effect. These have yet to be observed experimentally.

The magnitude of the alignment effect is illustrated in Fig. 12a for a single-neutron $\ell = 2$ knockout with theoretical single-particle cross sections of 12.5, 11.6, and 26.0 mb for states with m=0, 1, and 2, respectively. The unaligned, spin-averaged cross section is 17.6 mb. This m sensitivity suggests that, in experiments where the secondary beam has spin greater than 1/2 and was produced in a breakup process, it is entirely possible that some degree of spin alignment will be present in the beam. This could pose a source of systematic error on the absolute cross section. With this in mind, an exploratory theoretical study was carried out for the spin 3/2 ^{17}C system at 65 MeV/nucleon (116). This showed that the calculated analyzing powers T_{20} associated with the stripping process could indeed be significant. For an incident beam of alignment t_{20} then the cross section due to the aligned beam is

$$\sigma_{sp}(\text{aligned}) = \sigma_{sp}\left[1 + t_{20}T_{20}\right] \ , \tag{19}$$

where σ_{sp} is the usual, unaligned single-particle cross section. $T_{20}(0^+)$ for the pure $\ell = 2$, ^{16}C ground state transition was found to be 0.234 within the eikonal model. In the case of the mixed ℓ transition to the ^{16}C 2^+ state, see Fig. 1, the

calculated analyzing power is also of order 0.2. Furthermore, due to interference of the $\ell = 0$ and 2 contributions (116), $T_{20}(2^+)$ is sensitive to both the sign and the magnitude of the assumed admixtures. There is, as yet, no experimental evidence that bears on these questions, but they will provide a rich and necessary field for future studies.

The presence of tertiary beam alignment will also manifest itself through a non-isotropic emission of gamma rays from the reaction residues. As a specific example, consider neutron knockout from the 0^+ ground state of ^{28}Mg producing the $5/2^+$ state at 1.7 MeV in ^{27}Mg. To lowest order, the m_ℓ population of the residue will then correspond to the single-particle knockout cross sections calculated from Eqs. (7) and (8). Transforming these to the j alignment and using the expressions given in the reviews by Yamazaki (117) and, with special emphasis on fragmentation reactions, by Stuchberry (118), the theoretical angular distributions of gamma rays can be calculated. The results for the two examples in Fig. 12b show that the anisotropy is expected to be appreciable. It can be increased further by cuts in the momentum distribution. The cross-hatched area in Fig. 12a includes 38% of all events, but the anisotropy is then doubled. It is clear that the method has great potential for identifying the spins of residues and the associated gamma-transition multipolarities in knockout reactions.

The additional scale on the abscissa of Fig. 12b illustrates the strong effect of the Lorentz boost in a fast-beam knockout reaction. This can easily be incorporated in the analysis and does not, in principle, present any obstacle. The strong forward peaking implies that the angular detection range 0-60° will yield the highest count rates. However, at these forward angles, neutrons and charged particles generate a serious background in coincidence with the residues, and thus

a better determination of the anisotropy may come from laboratory angles near 150°. The price to be paid, at the energy of this example, is an approximately five-fold reduction in the count rate per unit detector solid angle when compared with measurements at the forward angles. An alternative method would be to determine the angular correlation of the gamma ray with respect to the recoil direction of the residue in the center-of-mass system. The reconstruction of this would be technically very demanding but also offer a very clear signature covering, in principle, the complete angular range, similar to the study of the neutron angular correlation from recoiling ^{10}Li* cited in Fig. 8.

Although beyond the scope of the present article, we mention for completeness the possibility to produce polarized nuclei using breakup reactions. Polarization here refers to different populations of the $+m$ and $-m$ magnetic sub-states. The seminal work of Asahi et al. (119) shows that this is achieved if the residues are collected off the incident beam direction. The momentum selection plays an important role (120); settings below and above the beam velocity typically give the largest values, the polarization changing in sign in between. In these experiments the residues were collected in a stopper and the polarization detected using the asymmetry of the beta emissions. Combined with nuclear magnetic resonance techniques the method is a powerful tool for measuring nuclear magnetic moments (121, 122). Breakup reactions must also be expected to produce alignment, although we do not possess the tools for predicting the magnitude of the effect. The observation of anisotropic angular distributions by Sohler et al. (123) for some gamma rays emitted from fragments with masses 40–45 following ^{48}Ca breakup at 60 MeV/nucleon provides a first qualitative indication of an alignment effect.

6 CONCLUDING REMARKS AND OPEN QUESTIONS

The field of direct reaction spectroscopy of rare nuclei, produced as weak, intermediate energy fragmentation beams, is still very young. Before offering a summary of what has been achieved so far, we enumerate a number of outstanding experimental and theoretical questions and challenges.

6.1 Open experimental and theoretical questions

1. In this article the emphasis has been on $p-sd$ shell nuclei where structure theory is advanced and sophisticated. This has been crucial for our understanding of the reliability of the reaction aspects of the analyses. Extending experiments into the $f-p$ shells, and maybe beyond, will be the logical next step. The corresponding mass region, approximately A=40–100, represents the cutting edge of modern shell-model theoretical predictions and a coordinated input of new and precise data will be both demanding and very rewarding.

2. Conclusions regarding the spectroscopic factor reduction factors R_s, ascribed to short-range correlations, are based on a small data set and must be regarded as only preliminary. More cases for configurations which are well understood (such as closed shell or halo systems) are needed to extricate these effects from those of long-range correlations. Experiments using calcium and nickel isotopes and their neighbors seem to be the logical starting point. Systematic measurements at several energies, maybe up to 1 GeV/nucleon, will be an important test of the accuracy and consistency of results. Theory provides some understanding of the R_s values of 0.5–0.65 observed for strongly bound orbitals. Can it also account for the values

closer to unity found for halo cases?

3. The two-nucleon knockout reaction needs and deserves much further effort, both experimentally and theoretically. Unlike single nucleon knockout, the structure and reaction dynamics are now entangled and the spectroscopy will be both richer and more complex to interpret. The initial experimental results are a considerable stimulus to develop an integrated shell-model and eikonal reaction theory methodology.

4. Alignment effects, both in the secondary beam and of the residues from knockout, pose a number of important questions. The model estimates of these effects discussed in this article have yet to be observed experimentally. How important are they and how can they best be exploited for beam and reaction diagnostics and for an enhanced spectroscopy?

5. Deviations from the eikonal reaction theory are expected and have already been observed in selected reactions. Further, precision studies of these effects, theoretically as well as experimentally, are important to understand quantitatively the limits with which cross sections, and hence absolute spectroscopic factors, can be cited, and to shed further insight into the reaction mechanisms.

6. A potentially serious problem is posed by the presence of isomeric final states of the residue, for which the coincidence method fails. It will become necessary to develop techniques that can "flag" these cases. Similarly, the related uncertainty of isomeric components in the incident secondary beam, and their poisoning of the single- and two-nucleon spectroscopic studies, will need to be addressed as a matter of importance.

7. A more systematic study of dynamical excitation of the residues, i.e. non-spectator effects, will also need to be carried out. Single-particle excitations are unlikely to play any significant role, however, collective (vibrational and rotational) excitations have already been suggested to be important in specific instances. A documented case (9) is the strength of the observed partial cross section of the ^{10}Be 2^+ state in neutron removal from ^{11}Be. Additional theoretical work must extend the reaction theory beyond the spectator core approximation.

6.2 Summing up

In recent years the single-nucleon knockout reaction has begun to be developed into a major, efficient tool for the spectroscopy of single-particle states in light and medium-mass nuclei produced as fast radioactive beams. The method has three essential technical elements, a fragment separator which delivers the exotic species of interest on a light target, a high-resolution spectrograph which identifies the reaction residues, and, operated in coincidence with this, an array of gamma-ray detectors which tag the individual residue excited state populations following the reaction. Based on this information, partial cross sections and their longitudinal momentum distributions can be measured. The technique is very sensitive; experiments have been carried out using incident beams with as few as one atom per second. The analysis of the spectral information uses a non-perturbative reaction theory, based on the sudden and eikonal approximations, and which requires a small, quite well determined parameter set. This permits orbital angular momentum assignments (from the shapes of the measured momentum distributions) and deduced spectroscopic factors (from the absolute

partial cross sections). The cases studied so far show consistent agreement between experiment and theory at a level which rivals that of classical light-ion transfer reactions at tandem accelerator energies.

Although based on a limited number of cases the new development, discussed in Sect. 4, indicates that the knockout method is able to determine absolute spectroscopic factors. It confirms the quenching factors R_s of 0.5–0.65 for deeply bound-proton states and obtains the same values for deeply-bound neutron states, a new but not surprising result. This reduction, relative to shell-model calculations with effective interactions, is taken to be a manifestation of the short-range repulsive force at short distances in the nucleon-nucleon interaction. It is interesting that the less-bound states of radioactive nuclei have R_s values much closer to unity. Another significant step forward is the identification of two-proton knockout from neutron-rich systems as a direct reaction. This process, and two-neutron knockout on proton-rich nuclei, is very interesting. It leads away from stability toward extremely rare nuclei, offering a sensitive probe of excited states and, potentially, of correlations in the many-body nuclear wave function. The practical exploitation of this coherence of the two-nucleon knockout mechanism is a challenge for future experiments and theoretical structure and reaction studies.

This work was supported by the U. S. National Science Foundation under grant No. PHY-01 10253 and by the United Kingdom Engineering and Physical Sciences Research Council (EPSRC) Grant No. GR/M82141.

Literature Cited

1. Brown BA, Wildenthal BH. Annu. Rev. Nucl. Part. Sci. 38: 29 (1988)
2. Brown BA. Prog. Part. Nucl. Phys. 47: 517 (2001)
3. Otsuka T, Honma M, Mizuzaki T, Shimizu N, Utsuno Y. Prog. Part. Nucl. Phys. 47: 319

(2001)

4. Honma M, Otsuka T, Brown BA, Mizuzaki T. Phys. Rev. C 61: 064609 (2000)
5. Pieper SC, Wiringa RB. Annu. Rev. Nucl. Part. Sci. 51: 53 (2001)
6. Glasmacher T. Annu. Rev. Nucl. Part. Sci. 48: 1 (1998)
7. Navin A et al. Phys. Rev. Lett. 81: 5089 (1998)
8. Tostevin JA. J. Phys. G 25: 735 (1999)
9. Aumann T et al. Phys. Rev. Lett. 84: 35 (2000)
10. Navin A et al. Phys. Rev. Lett. 85: 266 (2000)
11. Guimarães V et al. Phys. Rev. C 61: 064609 (2000)
12. Maddalena V et al. Phys. Rev. C. 63: 024613 (2001)
13. Tostevin JA. Nucl. Phys. A 682: 320c (2001)
14. Hansen PG, Sherrill BM. Nucl. Phys. A 693: 133 (2001)
15. Enders J et al. Phys. Rev. C 65: 034318 (2002)
16. Tostevin JA et al. Phys. Rev. C 66: 024607 (2002)
17. Brown BA, Hansen PG, Sherrill BM, Tostevin JA. Phys. Rev. C 65: 061601(R) (2002)
18. Enders J et al. Submitted to Phys. Rev. C
19. Esbensen H. In (62) p. 71 (1998)
20. Austin S. In (62) p. 42 (1998)
21. Austern N. *Direct Nuclear Reaction Theories* New York: Wiley (1970)
22. Macfarlane MH, Schiffer JP. In *Nuclear Spectroscopy and Reactions, Part B, ed. Cerny J*, p. 169. New York: Academic Press (1974)
23. Glendenning NK. In *Nuclear Spectroscopy and Reactions, Part D, ed. Cerny J*, p. 319. New York: Academic Press (1974)
24. Satchler GR. *Direct Nuclear Reactions* Oxford: University Press (1983)
25. Feshbach H. *Theoretical Nuclear Physics: Nuclear Reactions* p. 455. New York: Wiley (1992)
26. Johnson RC, Soper PJR. Phys. Rev. C 1: 976 (1970)
27. Harvey JD, Johnson RC. Phys. Rev. C 3: 636 (1971)
28. Kamimura M et al. Prog. Theor. Phys. Suppl. 89: 1 (1986)
29. Austern N et al. Phys. Rep. 154: 125 (1987)
30. Brown BA. *Some notes on Spectroscopic Factors* To be published

31. Dieperink AEL, de Forest T. Phys. Rev. C 10: 533 (1974)
32. Endt PM. Atomic Data and Nucl. Data Tables 19: 23 (1977)
33. Fortier S et al. Phys. Lett. B 461: 22 (1999)
34. Winfield JS et al. Nucl. Phys. A 683: 48 (2001)
35. Rehm KE et al. Phys. Rev. Lett. 80: 676 (1998); Nucl. Instr. Meth. A 449: 208 (2000)
36. Korsheninnikov AA et al. Phys. Rev. Lett. 82: 3581 (1999)
37. Mukhamedzhanov AM, Timofeuk NK. Pis'ma Zh. Eksp. Teor. Fiz. 51: 247 (1990)
38. Trache L, Carstoiu F, Gagliardi CA, Tribble RE. Phys. Rev. Lett. 87: 271102 (2001)
39. Xu HM, Gagliardi CA, Tribble RE, Mukhamedzhanov AM, Timofeuk NK. Phys. Rev. Lett 73: 2027 (1994)
40. Beaumel D et al. Phys. Lett. B 514: 226 (2001)
41. Gagliardi CA et al. Phys. Rev. C 59: 1149 (1999)
42. Typel S. To be published (2003)
43. Smith GR et al. Phys. Rev. C 30: 593 (1984)
44. Jacob G, Maris TAJ. Revs. Mod. Phys. 38: 121 (1966)
45. Kitching P, McDonald WJ, Maris TAJ. Vasconcellos CAZ. Adv. Nucl. Phys. 15: 43 (1985)
46. Kramer GJ, Blok HP, Lapikas L. Nucl. Phys. A 679: 267 (2001)
47. Pandharipande VR, Sick I, de Witt Huberts PKA. Revs. Mod. Phys. 69: 981 (1997)
48. Lapikas L, Wesseling J, Wiringa RB. Phys. Rev. Lett. 82: 4404 (1999)
49. Hansen PG. Nuclear Physics News 11: No. 4, 31-33 (2001)
50. Forsling W, Herrlander CJ, Ryde H (editors). *Proc. of the International Symp. on Why and How Should We Investigate Nuclides Far Off the Stability Line, Lysekil 1966*, Stockholm: Almqvist and Wiksell (1966); also as Arkiv for Fysik 36:1–686 (1967)
51. Tanihata I et al. Phys. Rev. Lett. 55: 2676 (1985); Phys. Lett. B 160: 380 (1985)
52. I. Tanihata (ed.). *Research Opportunities with Accelerated Beams of Radioactive Ions*, Nucl. Phys. A. 693: 1-513 (2001)
53. Kobayashi T et al. Phys. Rev. Lett. 60 :2599 (1988)
54. Orr NA et al. Phys. Rev. Lett. 69: 2050 (1992)
55. Bazin D, Caggiano JA, Sherrill BM, Yurkon J, Zeller A. Nucl. Instrum. Methods B, in press (2003)

56. Glauber RJ. In *Lectures in Theoretical Physics (W.E. Brittin ed.)*, Vol. 1, p. 315. New York: Interscience (1959)
57. Bertulani CA et al. *Physics of Radioactive Beams*, Nova Science Publishers Inc. (2002)
58. Thompson IJ, Suzuki Y. In (52)
59. Hansen PG, Jonson B. Europhys. Lett. 4: 409 (1987)
60. Hansen PG, Jensen AS, Jonson B. Annu. Rev. Nucl. Part. Sci. 45: 505 (1995)
61. Jonson B, Riisager K. Phil. Trans. R. Soc. Lond. A358: 2063 (1998)
62. Broglia RA, Hansen PG (editors). *International School of Heavy-Ion Physics, 4^{th} Course: Exotic Nuclei* Singapore: World Scientific, pp. 1–452 (1998)
63. Brown BA, Hansen PG. Phys. Lett. B 381: 391 (1996)
64. Hansen PG. In *Proceedings of the Int. Conf. on Exotic Nuclei and Atomic Masses, Arles, France, June 1995, ed. by de Saint Simon M, Sorlin O*, Orsay: Editions Frontières, pp. 175-186 (1995)
65. Hansen PG. Phys. Rev. Lett. 77: 1016 (1996)
66. Esbensen H. Phys. Rev. C 53: 2007 (1996)
67. Hardy JC, Carraz LC, Jonson B, Hansen PG. Phys. Lett B 136: 331 (1984)
68. Gottfried K. *Quantum Mechanics* New York: Benjamin, p. 113 (1966)
69. Bazin D et al. Phys Rev. C 57: 2156 (1998)
70. Hussein M, McVoy K. Nucl. Phys. A 445: 124 (1985)
71. Hencken K, Bertsch G, Esbensen H. Phys. Rev. C 54: 3043 (1996)
72. Al-Khalili JS, Tostevin JA, Thompson IJ. Phys. Rev. C 54: 1843 (1996)
73. Tostevin JA, Al-Khalili JS. Nucl. Phys. A 616: 418c (1997)
74. Anne R et al. Nucl. Phys. A 575: 125 (1994)
75. Aumann T, personal communication (2003)
76. Charagi SK, Gupta SK. Phys. Rev. C 41: 1610 (1990)
77. Ray L. Phys. Rev. C 20: 1857 (1979)
78. Kox S et al. Phys. Rev. C 35: 1678 (1987)
79. Renberg PU, Measday DF, Pepin M, Schwaller P, Favier B, Richard-Serre C. Nucl. Phys. A 183: 81 (1972)
80. Ozawa A, Suzuki T, Tanihata I. Nucl. Phys. A 693: 32 (2001)

81. Typel S, Baur G. Phys. Rev. C 50: 2104 (1994)

82. Warburton EK, Brown BA. Phys. Rev. C 46: 923 (1992)

83. Iwasaki H et al. Phys. Lett. B 481: 7 (2000); Phys. Lett. B 491: 8 (2000)

84. Datta Pramanik U et al. Phys. Lett. B 551: 63 (2003)

85. Cortina-Gil D et al. Phys. Lett. B 529: 36 (2002)

86. Sauvan E et al. Phys. Lett. B 491: 1 (2000)

87. Al-Khalili JS et al. Nucl. Phys. A 581: 331 (1995)

88. Esbensen H, Bertsch GF. Phys. Rev. C 64: 014608 (2001)

89. Esbensen H, Bertsch GF. Nucl. Phys. A 600: 37 (1995)

90. Brooke JM et al. Phys. Rev. C 59: 1560 (1999)

91. Tostevin JA et al. Prog. Theor. Phys. Suppl. 146 : 338 (2003)

92. Bonaccorso A, Brink DM. Phys. Rev. C 38: 1776 (1988)

93. Hasan H, Brink DM. J. Phys. G 4: 1573 (1978)

94. Bonaccorso A. Phys. Rev. C 60: 054604 (1999)

95. Bonaccorso A, Bertsch GF. Phys. Rev. C 63: 044604 (2000)

96. Tostevin JA et al. Phys. Rev. C 63: 024617 (2001)

97. Chen L, Blank B, Brown BA, Chartier M, Galonsky A, Hansen PG, Thoennessen M. Phys. Lett. B 505 (2001) 21.

98. Chartier M et al. Phys. Lett. B 510: 24 (2001)

99. Thoennessen M et al. Phys. Rev. C 59: 111 (1999) 111

100. Seth KK et al. Phys. Rev. Lett. 58: 1930 (1987)

101. Bohlen HG et al. Z. Phys. A 330: 227 (1988)

102. von Oertzen W et al. Nucl. Phys. A 588: 129c (1995)

103. Hansen PG. Nucl. Phys. A 682: 310c (2001)

104. Simon H. Phys. Rev. Lett. 83: 496 (1999)

105. Markenroth K et al. Nucl. Phys. A 679: 462 (2001)

106. Trache L, Carstoiu F, Mukhamedzhanov AM, Tribble RE. Phys. Rev. C 66: 035801 (2002)

107. Olson DL et al. Phys. Rev. C. 28: 1602 (1983)

108. Kidd JM et al. Phys. Rev. C. 37: 2613 (1988)

109. Miller KL et al. To be published

110. Schwab W et al. Z. Phys. A 350: 283 (1995)

111. Blank B et al. Nucl. Phys. A 624: 242 (1997)

112. Cortina-Gil D et al. Eur. Phys. J. A 10: 49 (2001)

113. Terry JR et al. To be published (2003)

114. Bazin D et al. Phys. Rev. Lett., submitted (2003)

115. Bohr Aa., Mottelson BR. *Nuclear Structure* (New York: Benjamin), Vol. 2, pp. 258-61, 641-6 (1975)

116. Johnson RC, Tostevin JA. *Spins in Nuclear and Hadronic Reactions* (Singapore: World Scientific): pp. 155-164 (2000)

117. Yamazaki T. Nuclear Data A3: 1 (1967)

118. Stuchbery AE. to be published in Nucl. Instr. Meth.

119. Asahi K et al. Phys. Lett. B 251: 488 (1990)

120. Okuno H et al. Phys. Lett. B 335: 29 (1994)

121. Mantica PF et al. Phys. Rev. C 55: 2501 (1997)

122. Rogers WF et al. Phys. Rev. C 62: 044312 (2000)

123. Sohler D et al. Phys. Rev. C 66: 054302 (2002)

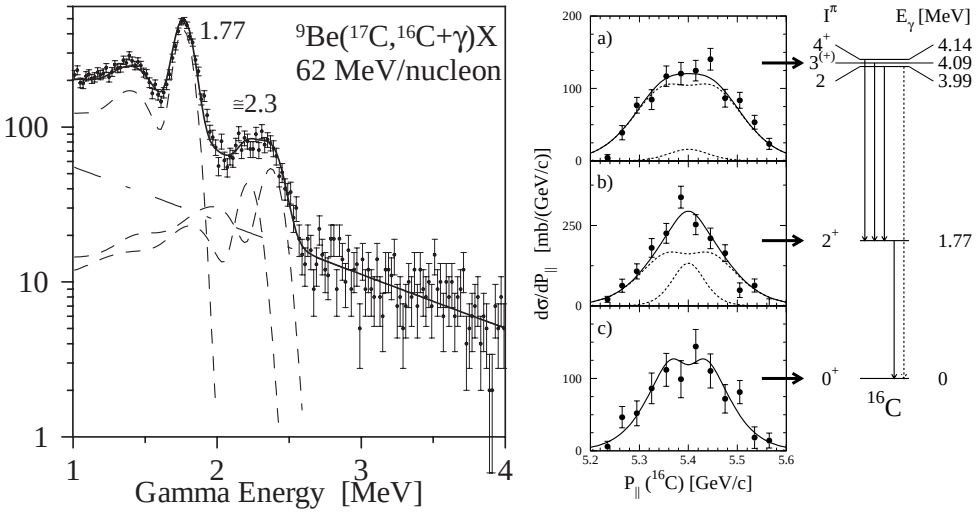

Figure 1: Neutron knockout from a ^{17}C beam. The left part of the figure shows the Doppler-corrected γ-ray spectrum observed in the ^{9}Be(^{17}C,^{16}C+γ)X reaction in coincidence with the reaction residues (12). The full-drawn curve is a fit to the spectrum based on simulated line shapes (dashed lines). The simplified level scheme on the right based on the γ-rays interprets the reaction as feeding (a) a group of states near 4 MeV, (b) the 2^{+} state at 1.77 MeV, with the and (c) the ground state of ^{16}C with cross sections of 33(7), 60(12) and 22(11) mb, respectively. The diagrams in the middle show the parallel-momentum distributions deduced from the γ coincidences, demonstrating that (a) and (c) are predominantly ℓ=2 (the broad components) while the cross section to the 1.77 MeV level has an appreciable ℓ=0 neutron component (the narrow component).

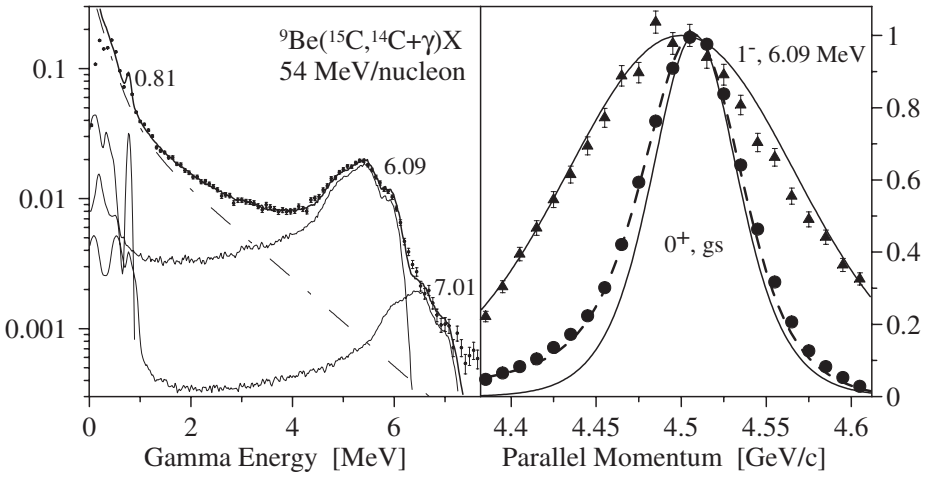

Figure 2: Knockout from the $1/2^+$ neutron halo nucleus ^{15}C. The Doppler-corrected γ-ray spectrum (a), observed in coincidence with ^{14}C reaction residues, shows that about 20% of the cross section leads to excited states. The dominant part is to a 1^- level at 6.09 MeV with the momentum distribution shown by the triangles in (b). Subtraction of the contributions from excited levels gives the momentum distribution of the cross section to the ground-state (circles), where the errors are smaller than the size of the points. The full-drawn curves are the parallel-momentum distributions calculated in eikonal theory for ℓ =0 and 1. The dashed line is the CDCC analysis discussed in subsection 3.5. (All distributions are shown in arbitrary normalization. From Ref. (16).)

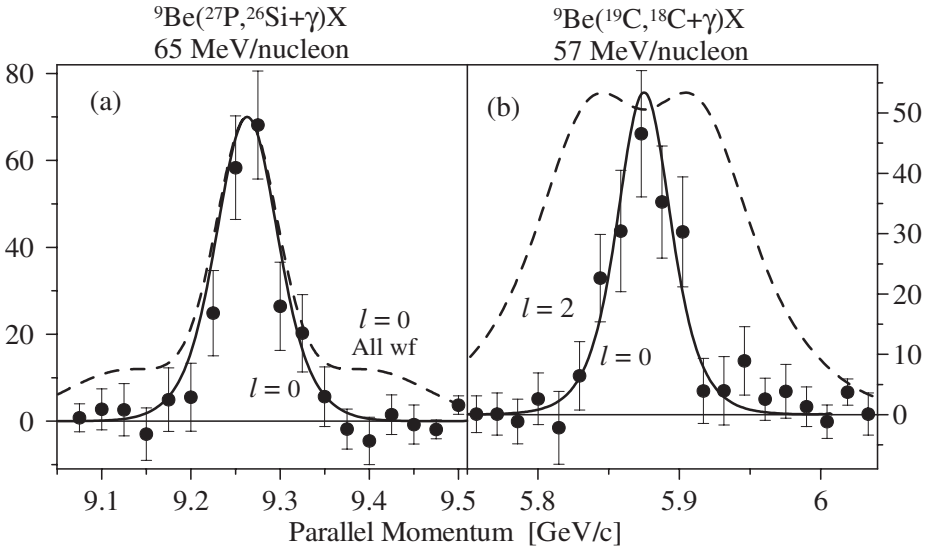

Figure 3: The momentum distributions for knockout to the 0^+ ground states obtained by subtracting the (predominantly ℓ=2) distributions to excited state by the method of tagging the coincidences integrally with all gamma rays above 0.25 MeV. The corresponding cross sections relative to the total are 30(10)% for the proton halo of ^{27}P and 56(9)% for the neutron halo of ^{19}C. The curves are theoretical calculations using eikonal theory. (All distributions are shown in arbitrary normalization). From Refs. (7, 12).

Table 1: Spectroscopic factors in the ^{9}Be(^{12}Be,^{11}Be)X reaction (10). The calculation of the experimental spectroscopic factors S_j is discussed in the text. We compare them with the shell model results obtained for a closed p-shell (labeled $0\hbar\omega$) and a calculation using the WBT interaction (82). For the latter it was assumed that the lowest $[0p]^8$ and $[0p]^6[1s,0d]^2$ 0^+ states in ^{12}Be are degenerate.

j^π	E	σ_{exp}	M	σ_{str}	σ_{dif}	σ_C	S_j		
	(MeV)	(mb)		(mb)	(mb)	(mb)	exp.	WBT	$0\hbar\omega$
$1/2^+$	0	32.0(47)	0.79	55.3	24.6	0.8	0.50(7)	0.61	0.0
$1/2^-$	0.32	17.5(26)	0.83	36.7	13.0	0.3	0.42(6)	0.99	2.18
$5/2^+$	1.8	-	-	37.1	12.6	-	-	0.48	0.0

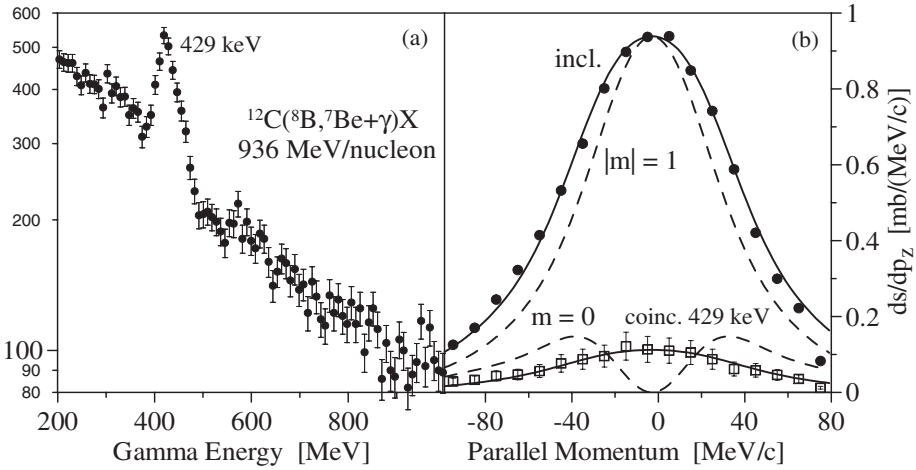

Figure 4: Knockout from the proton halo nucleus ^{8}B at 936 MeV/nucleon. The Doppler-corrected γ-ray spectrum (a), in coincidence with the reaction residues, shows that 13(3)% of the cross section goes to the ^{7}Be $1/2^{-}$ excited state. The coincident and inclusive momentum distributions (b) agree well with the parallel-momentum distributions calculated in eikonal theory for ℓ =1 shown as full-drawn lines. The dashed lines show the relative contributions of $|m|$=0 and 1 to the inclusive spectrum. From Ref. (85).

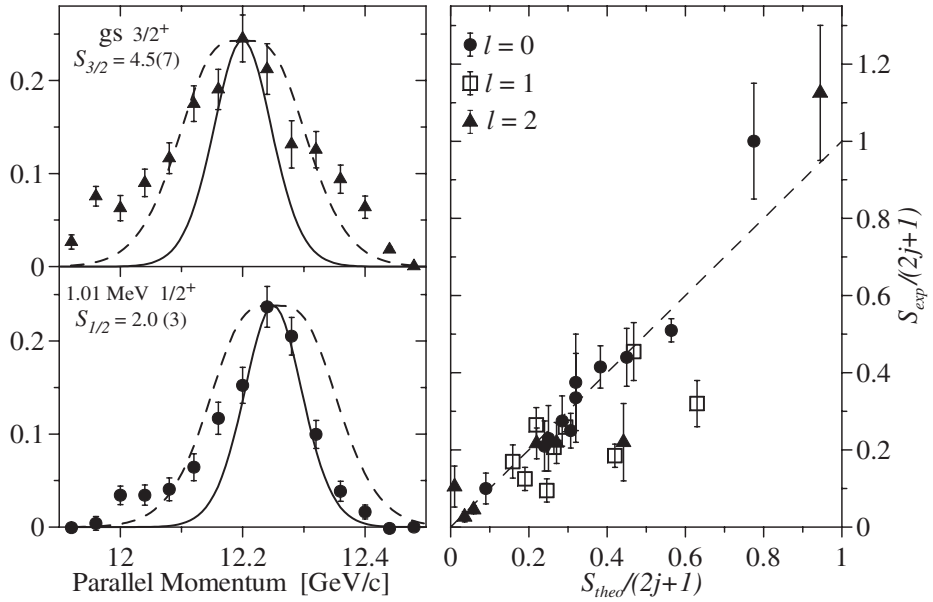

Figure 5: Parallel-momentum distributions (left) of the reaction residues in the (^{34}Si,^{33}Si) neutron knockout reaction obtained from γ-coincidence data (15). Theoretical, eikonal approximation (65) estimates are shown for $\ell = 0$ (solid) and $\ell = 2$ (dashed). The heights and centroids of the theoretical curves have been scaled to match the data. Experimental versus theoretical spectroscopic factors (right) in units of the sum-rule value $(2j + 1)$. The dashed line is the diagonal. The two, basically unrelated, quantities are seen to be correlated with a scale factor of approximately unity.

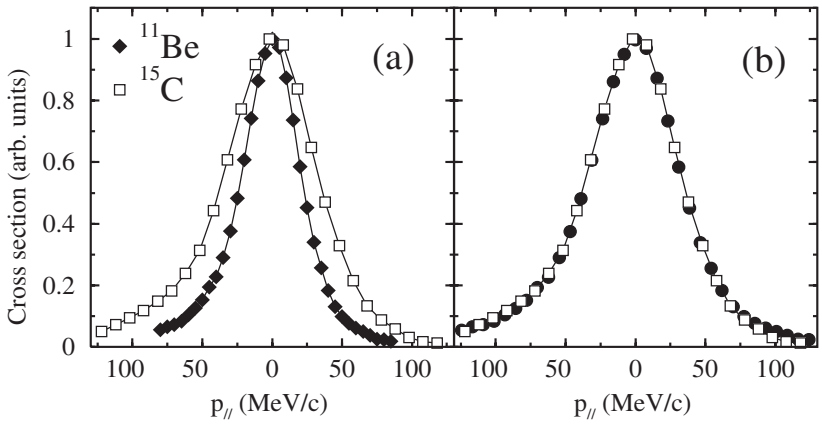

Figure 6: Comparison of (a) the measured parallel momentum distributions, in the projectile rest frame, for the ground state to ground state transitions in neutron removal from ^{11}Be (filled diamonds) and ^{15}C (open squares) at energies of 54 and 60 MeV/nucleon, respectively. The lines are a guide to the eye. In (b) the filled circles show the result of scaling the width of the ^{10}Be distribution by the square root of the ratio of the separation energies, $\sqrt{1.218/0.503}$, an illustration of the scaling relationship discussed in connection with Eqs. (9) and (10). (From Ref. (16).)

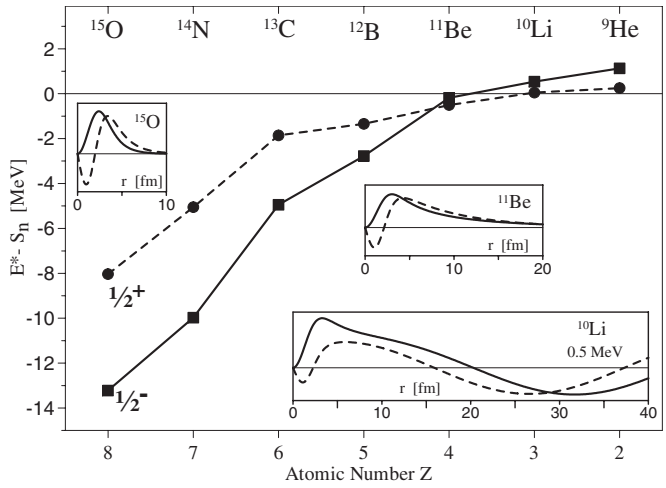

Figure 7: Systematics of the eigenenergies of the $1/2^+$ (circles, dashed) and $1/2^-$ (squares, full drawn) states as a function of the proton number for the N=7 isotones. The effective single particle energy is taken as the difference between the nuclear excitation energy and the ground state neutron separation energy. In ^{15}O with one neutron hole in the 8-8 doubly-closed shell, the $1/2^+$ state belonging to the next (*sd*) shell is 5 MeV above the $1/2^-$ ground state. The two states approach each other with decreasing proton number. In ^{11}Be they have crossed so that the $1/2^+$ intruder is the ground state, and the s and p states are bound by only 0.50 and 0.18 MeV, respectively. Both are halos with radii close to 7 fm. (The core radius is 2.3 fm.) The same states have been observed (97, 99–102) as continuum states in the unbound nuclei ^{10}Li and ^{9}He. The insets show the calculated single-particle wave functions as plots of $\chi(r) = rR(r)$ against r calculated for a Woods-Saxon potential. Both states are deeply bound with spatially well-localized wave functions in ^{15}O, they are halos in ^{11}Be, and continuum wave functions in ^{10}Li (shown for a kinetic energy of 0.5 MeV) and ^{9}He.

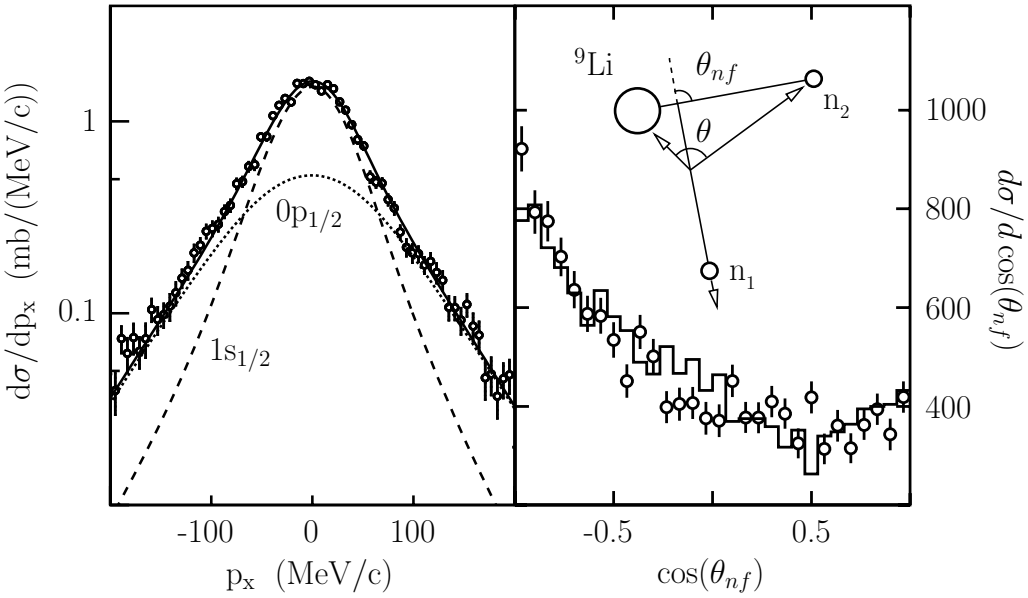

Figure 8: ^{10}Li residue momentum distributions (left) measured following neutron removal from ^{11}Li on a ^{12}C at 287 MeV/nucleon. Angular correlations of the decay neutrons (right) measured relative to an axis defined by the ^{10}Li recoil direction as shown in the inset. The points are the experimental data and the histogram is a reconstruction corrected for experimental resolution and acceptance effects. Note the strong forward-backward asymmetry, which reflects interference of the ℓ=0 and 1 final states. (From Simon *et al.* (104).)

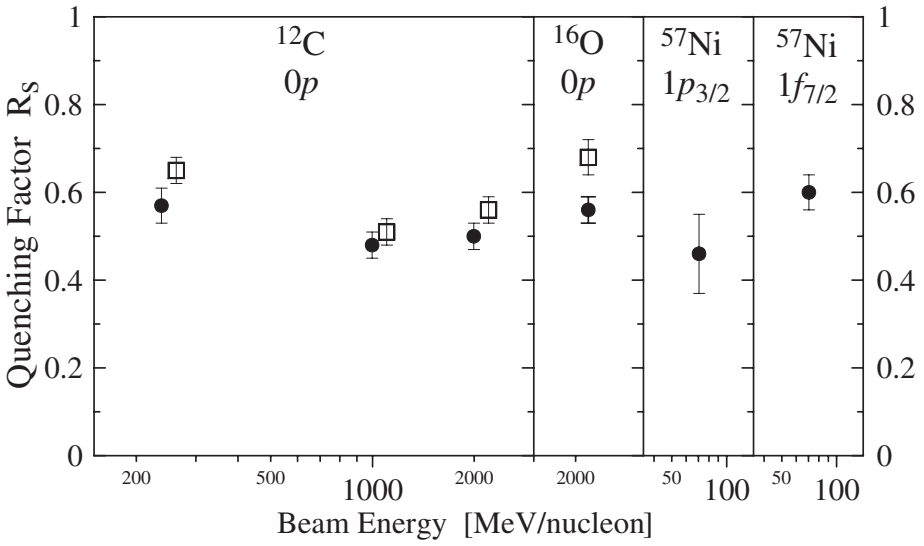

Figure 9: Systematics of the reduction factor R_s, attributed to short-range correlations, for the isotopes ^{12}C and ^{16}O (17) based on data from (107, 108), and for ^{57}Ni (109). The reactions leading to the final states have nucleon separation energies in the range 10–19 MeV. The open squares are the results for proton knockout while the full circles are for neutron knockout. The ^{57}Ni experiment used a beryllium target, while the other experiments used a carbon target. The measurements, except for the $1p_{3/2}$ state of ^{57}Ni, are inclusive.

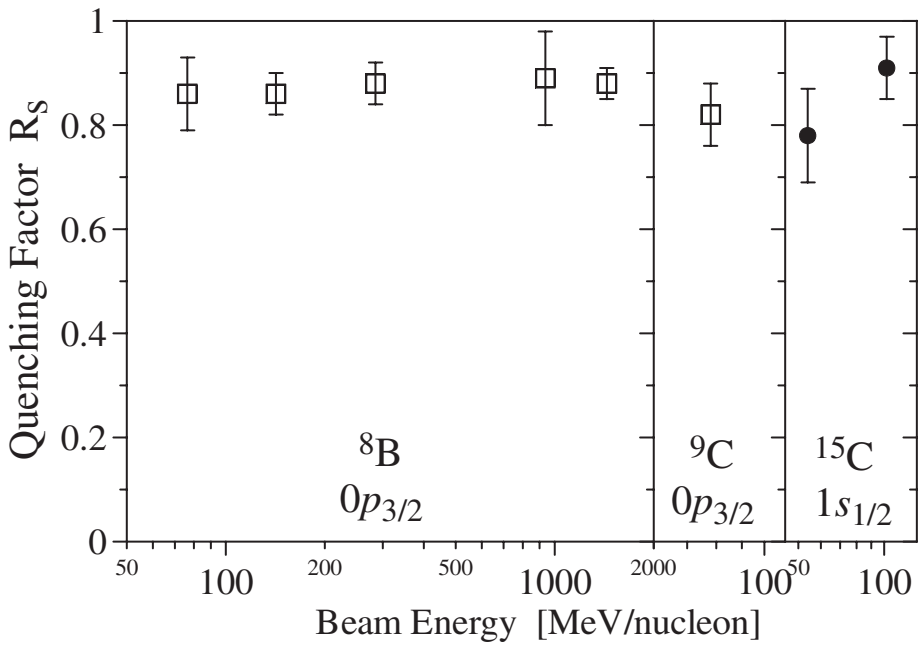

Figure 10: Systematics of the reduction factor R_s, attributed to short-range correlations, for the isotopes ^{8}B (17) with data from (85,110–112), ^{9}C (18), and ^{15}C (113). The final states have nucleon separation energies in the range 0.14–1.3 MeV. The open squares are the results for proton knockout while the full circles are for neutron knockout. The ^{15}C experiment used a beryllium target, the others carbon targets. The measurements for ^{8}B are inclusive, but a recent experiment (85) has found that the branch to the ^{7}Be excited level is 13±3% in agreement with the theoretical calculation, see Fig. 4.

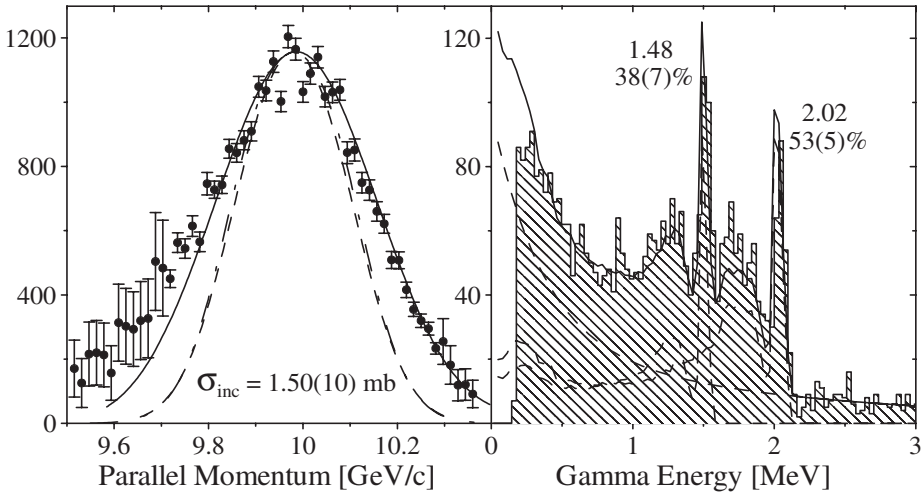

Figure 11: The left part of the Figure shows the parallel-momentum distribution for the inclusive two-proton knockout reaction from ^{28}Mg. The theoretical curves are discussed in the text. They include the broadening arising from the difference in stopping power in the target for projectile and residue. The full drawn curve is the estimate for knockout of two protons in $0d$-states, while the dashed lines are for two protons in $1s$-states and for knockout of a single $0d$ proton. The latter is indicative of one-proton removal mechanisms. The right part of the Figure shows the gamma-ray spectrum (in units of counts per 32 keV bin). The main peaks are labeled by the energy in MeV (error 0.02 MeV) and by the absolute intensity relative to the number of observed fragments. The dashed peak shapes are simulated response curves normalized to match the number of counts in the full-energy peaks. The continuous distribution (dashed line) is attributed to radiation from the target. The 1.48 MeV and 2.02 MeV peaks are interpreted as originating from the 4^+ and 2^+ levels of ^{26}Ne, respectively.

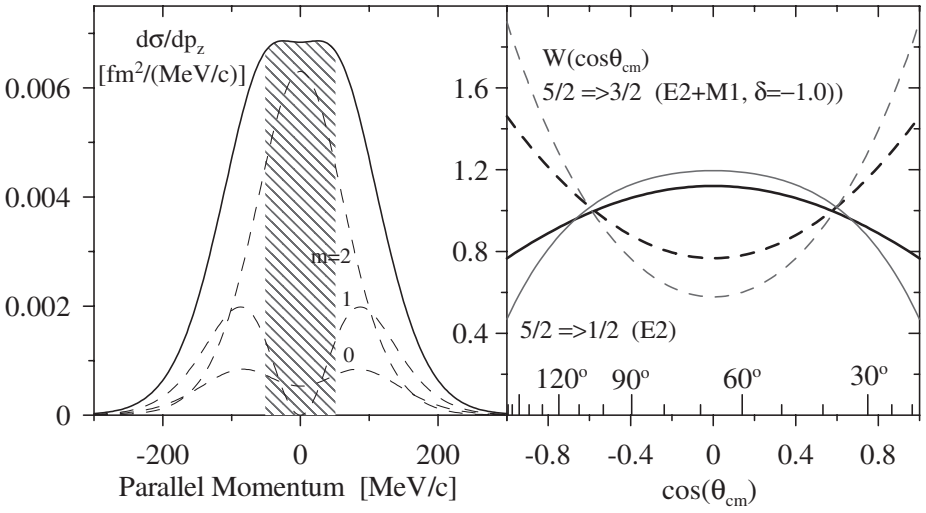

Figure 12: The left panel shows the calculated longitudinal momentum distribution for the knockout of a $0d_{5/2}$ neutron in the ^{9}Be(^{28}Mg,^{27}Mg)X reaction at 82 MeV/nucleon. The dashed lines give the contributions of the individual m_ℓ magnetic sub-states. A cut of $\pm$50 MeV/c increases the contribution of $m_\ell = \pm 2$ from 59 to 84% with 38% of the intensity included. The right panel shows the calculated angular distributions for two possible spin sequences from the $\frac{5}{2}^+$ excited state of the residue. The gamma-ray angle relative to the beam axis in the center-of mass frame is denoted θ_{cm}. The heavy lines are for coincidences with all residues. The anisotropy is almost doubled (thin lines) by selecting central momenta of the cross-hatched area in (a). The upper scale on the x-axis shows the corresponding laboratory angles for a beam energy of 82 MeV/nucleon.